AD-A113 782 GEORGIA INST OF TECH ATLANTA SCHOOL OF PHYSICS F/G 11/6
ION IMPLANTATION STUDIES OF TITANIUM METAL SURFACES.(U)
1981 J R STEVENSON, K O LEGG, M W RIBARSKY AFOSR-79-0011
UNCLASSIFIED AFOSR-TR-82-0327 NL

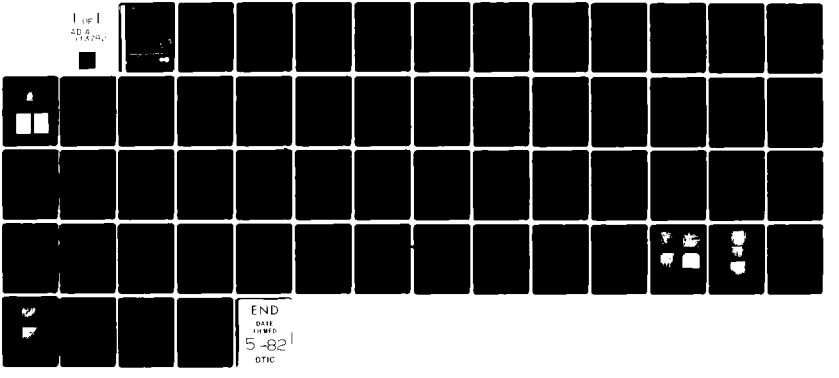

END
DATE FILMED
5-82
DTIC

(10)

FINAL REPORT

ION IMPLANTATION STUDIES OF TITANIUM METAL SURFACES

By

James R. Stevenson
Keith O. Legg
Martin W. Ribarsky

pared for

R FORCE OFFICE OF SCIENTIFIC RESEARCH
LLING AFB, BLDG. 410
SHINGTON, D.C. 20332

der

ntract No. AFOSR–79–0011

Final Report Period Covered from November 1, 1978 to October 31, 1981

GEORGIA INSTITUTE OF TECHNOLOGY
A UNIT OF THE UNIVERSITY SYSTEM OF GEORGIA
SCHOOL OF PHYSICS
ATLANTA, GEORGIA 30332

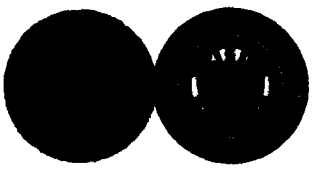

ION IMPLANTATION STUDIES OF TITANIUM METAL SURFACES

Unclassified

SECURITY CLASSIFICATION OF THIS PAGE (When Data Entered)

REPORT DOCUMENTATION PAGE		READ INSTRUCTIONS BEFORE COMPLETING FORM
1. REPORT NUMBER AFOSR-TR- 82-0327	2. GOVT ACCESSION NO. AD-A113 782	3. RECIPIENT'S CATALOG NUMBER
4. TITLE (and Subtitle) Ion Implantation Studies of Titanium Metal Surfaces.		5. TYPE OF REPORT & PERIOD COVERED Final 6. PERFORMING ORG. REPORT NUMBER
7. AUTHOR(s) James R. Stevenson Keith O. Legg Martin W. Ribarsky		8. CONTRACT OR GRANT NUMBER(s) AFOSR-79-0011
9. PERFORMING ORGANIZATION NAME AND ADDRESS Georgia Institute of Technology School of Physics, Atlanta, GA. 30332		10. PROGRAM ELEMENT, PROJECT, TASK AREA & WORK UNIT NUMBERS 61102F 2303/A3
11. CONTROLLING OFFICE NAME AND ADDRESS Air Force Office of Scientific Research/NC Bolling AFB, Bldg, 410 Washington, D. C. 20332		12. REPORT DATE 1981 13. NUMBER OF PAGES 59
14. MONITORING AGENCY NAME & ADDRESS(if different from Controlling Office)		15. SECURITY CLASS. (of this report) Unclassified 15a. DECLASSIFICATION/DOWNGRADING SCHEDULE

16. DISTRIBUTION STATEMENT (of this Report)

Approved for public release;
Distribution unlimited.

17. DISTRIBUTION STATEMENT (of the abstract entered in Block 20, if different from Report)

18. SUPPLEMENTARY NOTES

19. KEY WORDS (Continue on reverse side if necessary and identify by block number)

Titanium, ion-implantation, grain growth, erbium surface segregation, Rutherford backscattering, infrared, laser, synchrotron, oxidation, electron energy loss.

20. ABSTRACT (Continue on reverse side if necessary and identify by block number)

The influence of implants on the surface characteristics and oxidation of titanium and the use of various techniques to probe the surface structure have been studied. The surface condition of the metal was shown to affect greatly the implant distribution. Erbium implants did not segregate at all to a clean titanium surface but segregated completely to a carbon covered surface. Initial monolayer oxide formation is unaffected by implanted calcium, which does not segregate to the surface. The electronic structure of the oxide layer is,

DD FORM 1 JAN 73 1473

Unclassified

SECURITY CLASSIFICATION OF THIS PAGE (When Data Entered)

however, unexpectedly complicated, showing features in the electron energy loss spectrum very different from the clean surface. It is shown that care must be taken in studying the loss spectrum itself, especially in identifying the plasmon loss peaks and features associated with the clean surface. It has been found that different implants can seriously affect mechanical strain in the oxide, leading to rumpling and spalling in the case of Ti or Sb implants. These effects appear to be associated with implant segregation to the metal-oxide interface. A semi-quantitative electron channeling method has been developed for determining damage levels in implanted materials.

The use and feasability of synchrotron radiation as an infrared source in new national facilities now under construction has been studied. The use of a far infrared wave-guide laser for probing the structure and kinetics of oxides was also studied.

Tables of Contents

I. Research Objectives

The long range objective of this research has been a basic approach to the study of high dose ion implantation in titanium, aluminum and alloys of Ti-Aℓ. The study has included determination of the depth profile of the implanted species and the kinetics of this profile with temperature cycling and grain size changes as well as during oxide and nitride formation. The growth kinetics of oxide and nitride formation was followed in ion implanted specimens to identify important controlling mechanisms. A new method for measuring radiation damage associated with the implantation process was developed and used to evaluate the effect of damage on growth kinetics and grain size distribution.

Other methods and techniques were used or developed to study the properties of the implanted materials. A far infrared waveguide laser was obtained and used to provide a more precise probe of the oxide formation on titanuim surfaces. In addition electron energy loss measurements were made on clean and oxidized titanium surfaces and the technique itself was studied.

In the following sections, we will present a detailed discussion of how we met our objectives. In the next section a discussion of the general techniques used or developed in the course of this study is given. Following that the results using the techniques are reported.

II. General Techniques

Numerous established techniques have been used and new ones developed in the course of this study.

Implantations were carried out using a 200 keV commercial semiconductor ion implanter, either in its standard high vacuum chamber ($\sim 10^{-6}$ Torr) or in an ultra high vacuum chamber (base pressure 10^{-10} Torr; 10^{-9} Torr during implantation). annealing and oxidation has been carried out in a flowing gas tube furnace.

Oxide thicknesses were measured by Rutherford backscattering in the medium energy regime readily available to us, using a silicon barrier detector. Oxide crystallography has been determined by a "pin-hole camera" x-ray technique, while Debye-Scherrer powder photography has been used for determining the bulk oxide crystallography. A technique has been developed for quantifying damage in the surface region using electron channeling in the scanning electron microscope.

Metallographic work for grain growth studies has used standard techniques of metallurgical etching and microscopic examination. Transmission electron microscopy, scanning electron microscopy, channeling contrast scanning and scanning Auger microscopy have been used for various aspects of this work.

Auger spectroscopy (AES), scanning Auger microscopy (SAM) and electron energy loss spectroscopy (EELS) have all been carried out in the UHV implantation chamber using a commercial cylindrical mirror electron energy analyzer (CMA).

An attempt has been made to develop a far infrared waveguide laser method of reflectivity determination for examining the electronic structure of oxides. This has been found to be possible only with a cost and complexity far in excess of the scope of this program.

Theoretical techniques have been developed for investigating the use of synchotron radiation in the far infrared and for analyzing FIR reflectivity spectra. Considerable progress has been made in carrying out cluster calculations using an X-alpha technique and in predicting the segregation of implants.

III. Effects of Erbium Implantation on Grain Growth

It is well known that titanium, in common with many other metals is subject to grain growth on annealing. During oxidation this would be a problem since it would change the grain boundary area available for oxygen diffusion. Since erbium is known to stabilize grain size in bulk titanium[1], we have investigated the possibility of using implanted Er to achieve the same effect with the surface grains.

The experiment consisted of examining the grain sizes in a number of Ti specimens, both pure and Er implanted to 5×10^{15} ion cm^{-2}, after different annealing times in an inert gas furnace at 750°C. All acquired a thin oxide film after 9 hrs., and on etching and metallographic examination none showed any increase in surface grain size over the starting material. In all samples, the bulk grains had increased five to ten times in diameter. It appeared that the stabilization of the surface grains came about either because of the slight oxidation or from some property unique to the surface, such as residual polishing strain, the breakdown in three dimenensional symmetry or the different surface energy term for a surface grain's energy balance. A similar annealing experiment was carried out in UHV, resulting in both bulk and surface grain growth at the same rate. Therefore surface oxidation itself stabilized the grains, rendering grain growth unimportant in this work.

During the course of this study another effect was noted which has considerable significance for work in this area. Af first it was found that Er implanted under standard high vacuum conditions segregated to the surface and diffused rapidly across the entire specimen even at low annealing temperatures (150°C). When Er was implanted in UHV or in cleaner HV, however, this did not occur, even at higher temperatures. Under all conditions an 18 hr. anneal at 750°C was required to obtain detectable diffusion of the implant into the bulk.

Theoretical analysis suggests that surface segregation occurs by diffusion up the carbon concentration profile which results from hydrocarbon cracking and knock-on in a standard oil pumped vacuum system. Clearly, a surface segregated implant

may have an effect on such properties as oxidation rates very different from that to be expected from a static implant. The fact that this segregation is dependent upon the cleanliness of the vacuum chambers makes measurements of implant profiles very important and shows the necessity of working under clean vacuum conditions.

The details of this work are given in Appendix (i) and discussed further in Sec. V.

IV. Oxide Growth

The growth of the oxide layer has been followed from the initial sub-monolayer absorption to the formation of scales several hundred nanometers thick. Antimony and cesium were chosen as examples of implants which respectively increase and decrease oxidation in titanium. They are similar in mass, and therefore in the extent of damage they produce, and both are heavier than titanium, making it possible to obtain density profiles by RBS.

Sub-monolayer oxide growth has been studied by AES for pure and Ca-implanted clean Ti. When Ca was implanted in UHV at 100 keV to a dose of 10^{15} ion cm^{-2}, no Ca was detectable on the surface. The sub-monolayer oxide growth kinetics were unaffected by the implant or any associated damage when exposure was made to 10^{-7} Torr of O_2 at 650°C This is shown by the oxygen uptake curves of fig. 4.1.

The RBS profiles of titanium after implantation and after subsequent oxidation are shown in Fig. 4.2. The ranges for Sb and Cs are both about 230 Å, somewhat smaller than the 300 Å expected from LSS theory. Both HV and UHV implants show the same profiles. After oxidation, however, it can be seen that the Cs implant density has been reduced by an order of magnitude while the Sb has almost disappeared. There is no evidence, however, of a diffusion profile into the bulk. Therefore the implant has not simply diffused away, and it seems most likely that it has moved to the metal -oxide interface.

After a 3hr. oxidation the implanted regions of the Sb-and Ti- implanted samples appeared milky, while outside the implanted regions they were a smooth blue-gray, as were the Cs-implanted and unimplanted samples. SEM examination showed smooth oxides in the unimplanted and Cs-implanted samples, whereas the surfaces of the Sb-and Ti-implanted samples were rumpled on a scale much smaller than the grain size. Indeed,on these samples the oxide layer readily cracked and spalled. (See fig. 4.3).

Pinhole x-ray diffraction showed that in all cases the oxide was tetragonal TiO_2. The x-ray data are shown in Fig. 4.4. The outer two rings are the Ti (011) and (012) reflections and show considerable granularity with some damage in implanted regions.

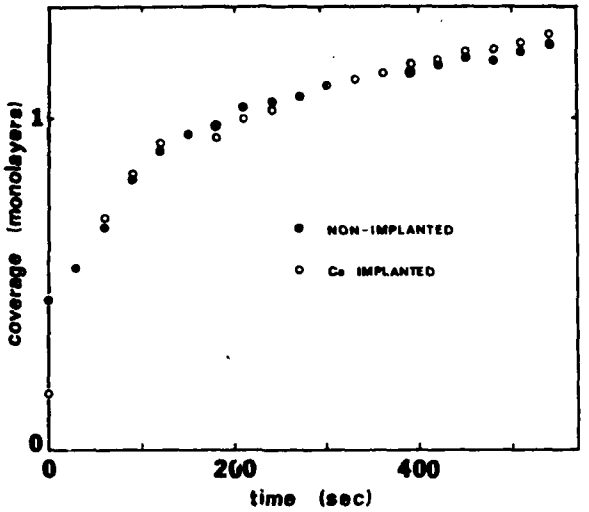

Fig. 4.1 Oxygen uptake for pure Ti and Ti implanted with 10^{15} ion cm^{-2} of Ca heated at 650 C in 10^{-7} Torr of oxygen.

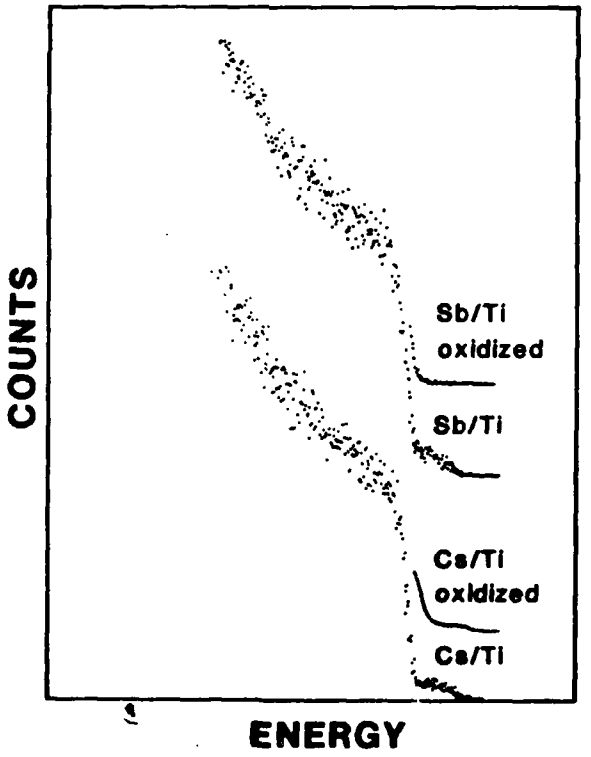

Fig. 4.2 Rutherford backscattering spectra from implanted and oxidized Ti using 180 keV He .

The inner ring is the TiO_2 (110) reflection. This has no discernable grain structure, showing that the oxide has a small grain size.

Clearly the damage, probably in the form of vacancy loops[2], is detrimental to the adhesion of the oxide, perhaps because the induced tensile strain[3] increases the mismatch between the metal and its oxide. Sb^+ is a smaller ion than Ti^{+3} and will therefore exacerbate the mismatch. Cs, however, being larger,[4] should reduce the strain, or even impose a compressive strain, if it remains at the metal-oxide interface.

Attempts at measuring the oxide thickness by RBS were largely unsuccessful. This was due to the fact that using He_4^{++} placed the oxygen signal at too low an energy, where the background began to rise steeply, whereas H^+ placed it at too high an energy, where the O edge became too close to the Ti edge. In future work He_3^{++} will be used.

Fig. 4.3 Scanning electron micrograph of Ti-implanted Ti showing rumpled and spalled oxide.

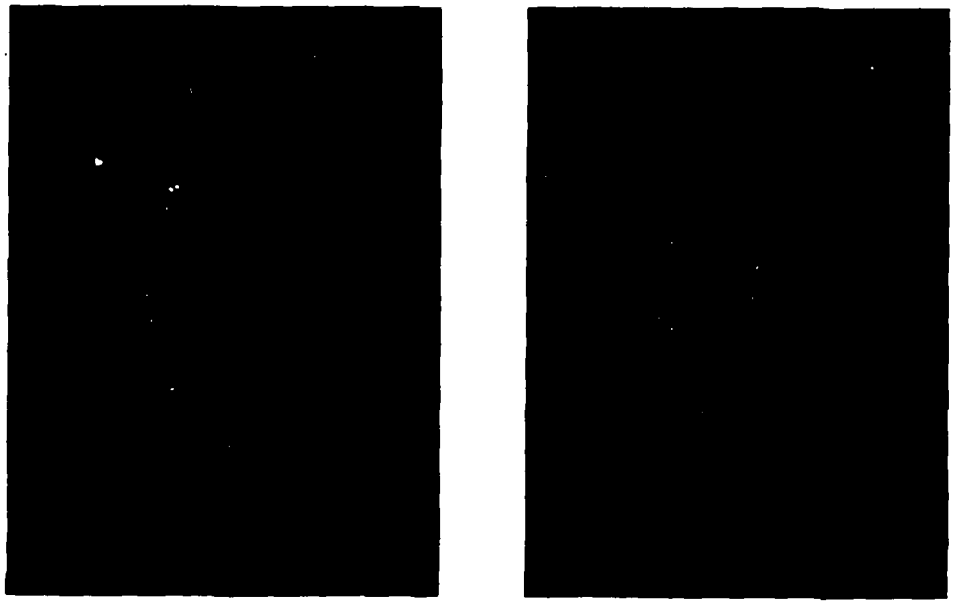

Fig. 4.4 Pinhole x-ray diffraction patterns from oxidized Ti.

V. Effects of Environment on the Implant Distribution

Most implantation done for industrial or technical use is carried out in a standard vacuum environment. On the other hand, in the basic research laboratory implanted materials may be made under rigorously clean conditions of high vacuum. We have found that there are significant differences between the implant profiles from these two environments for Er in Ti.

The standard vacuum produces a carbon covered Ti surface. The Er segregates to the carbon covered surface but not to the clean one. The Er, which peaks at a depth of about 350 Å in the clean Ti, shows a pronounced surface layer of no more than 100 Å thickness for the carbon-covered Ti. Auger analysis reveals no Er at the carbon surface suggesting that the implant segregated at the Ti/C interface or in a narrow Ti/C mixed region created by the bombardment. An analysis based on a pair-bonding approach to surface segregation in alloys indicates that the Er segregation may be due to stronger bonding of Er-C than Ti-C. The analysis also indicates that Er would segregate to the surface of an Er-C system. The details of the experimental results and of the analysis are presented in Appendix (i).

The obvious importance of differences due to surface conditions on implant distributions and perhaps in implant-substrate interactions is that the properties of the implanted material can change. Results for various surface conditions can also indicate changes that may take place at other interfaces-for example, at grain boundaries in the presence of certain impurities.

VI. Electron Energy-Loss Structure of Clean and Oxidized Titanium

The characteristic energy loss structure of a material provides a direct measure of the contributions from interband transitions and collective modes such as plasmons to the electronic excitation spectrum. The loss structure is altered by changes in bulk properties and also by surface modification or adsorption which acts particularly on certain features. An understanding of the behavior of surface and bulk plasmon modes especially is important for the use of loss spectra to study the effects of adsorption and ion implantation.

Unfortunately there is qualitative disagreement between the experimental loss spectra, and in addition the results have been given different interpretations so that very different energies for plasmons and interband transitions have been reported. The discrepancies in measurements on transition metals make it unclear whether the plasmon energy position is given by free-electron theory or whether something such as band structure effects is important. To clear up the confusion and also to provide a basis for use of EELS as a surface analysis tool, we made several measurements of the loss spectra for Ti systems.

The samples analyzed were polycrystals which were either clean or subjected to controlled amounts of oxygen exposure. The EELS results were consistent with those of Simmons and Scheibner[5] for samples prepared by thermal evaporation from pure metals. We carried out all measurements in a vacuum chamber with base pressure of 10^{-10} Torr. The samples were cleaned by argon bonbardment and not annealed, and Auger spectra showed less that ¼ monolayer of O on their surfaces with no C or S. The clean surface data was taken while sputtering so that there was no N build-up,especially from the pumps.

A single-pass CMA analyzed the spectra with a .3% E resolution in the direct counting mode. Unfortunately our Tracor-Northern multichannel analyzer had some noise, so the spectra were somewhat degraded from the best possible results.

The characteristic loss structure measurements fall into two classes: Measurements of losses suffered by electrons with energies of many kilovolts as they are

transmitted through thin films and measurements of losses suffered by electrons with energies around 100eV as they are reflected from the material. The former experiments are dominated by electrons which do not undergo elastic scattering while the latter are more highly resolved but contain electrons which have been elastically scattered at least once. The two types of spectra for evidently clean Ti surfaces are shown in Fig.6.1.[5,6] There are large qualitative differences between the spectra at energy losses below 20eV, especially between the lower reflection spectrum and the transmission spectrum. The data from our measurement for clean Ti, which is a reflection measurement, is shown in Fig. 6.2. It is more highly resolved than the reflection data in Fig. 6.1a, but it is qualitatively in agreement with it.

Our analysis of the clean Ti data is as follows. The peak around 5eV is undoubtedly a surface peak since it is quite sensitive to surface contamination and since it is less pronounced for higher primary electron energies as shown in Fig. 6.1a and 6.3. The latter behavior is consistent with a surface excitation since the mean free paths of the primary electrons are greater at higher energies which means the bulk signal would be enhanced with respect to the surface. We have identified this peak tentatively as a surface plasmon in agreement with Simmons and Scheibner[5] (SS) since collective modes should be more prominent at this energy relative to interband excitations. However, we need to confirm this identification with further measurements and analysis of how the intensity of this peak changes as the scattered electrons deviate from the specular direction. An intensity maximum at an angle away from the specular direction would indicate that the peak is a surface plasmon.[7] The prominent peak at about 10eV is the volume plasmon. The structure extending below this peak for about 20eV probably contains the second volume and surface-volume contributions postulated by SS, though our higher resolution data shows this structure to be less prominent than theirs. However, we also find a double peak at about 35eV which also appears in the appropriate place in measurements we have done on Fe, and we identify this as the split $(\frac{1}{2}, \frac{3}{2})$ Ti 3p interband excitation.

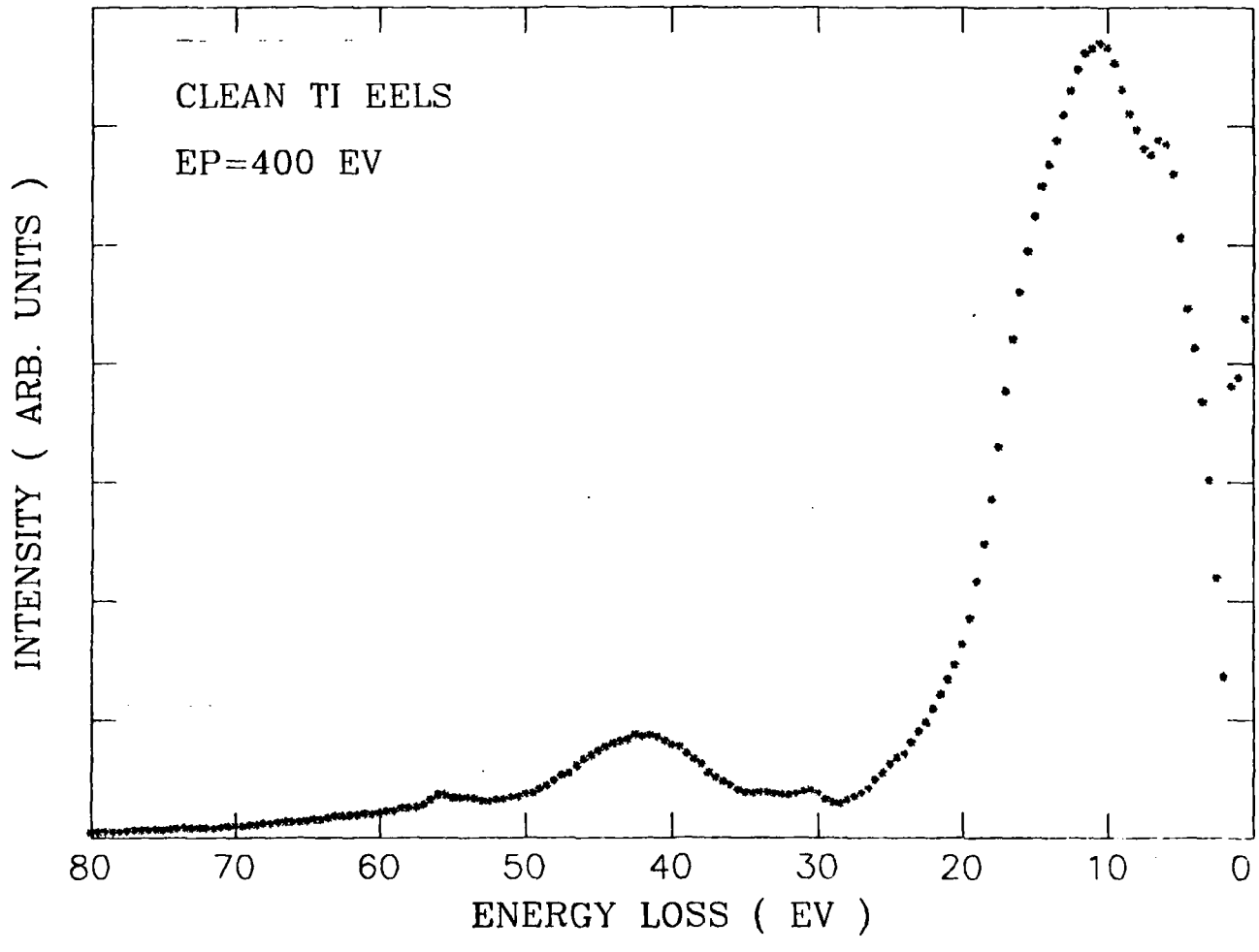

Fig.6.2 Clean Ti Energy Loss Spectrum.

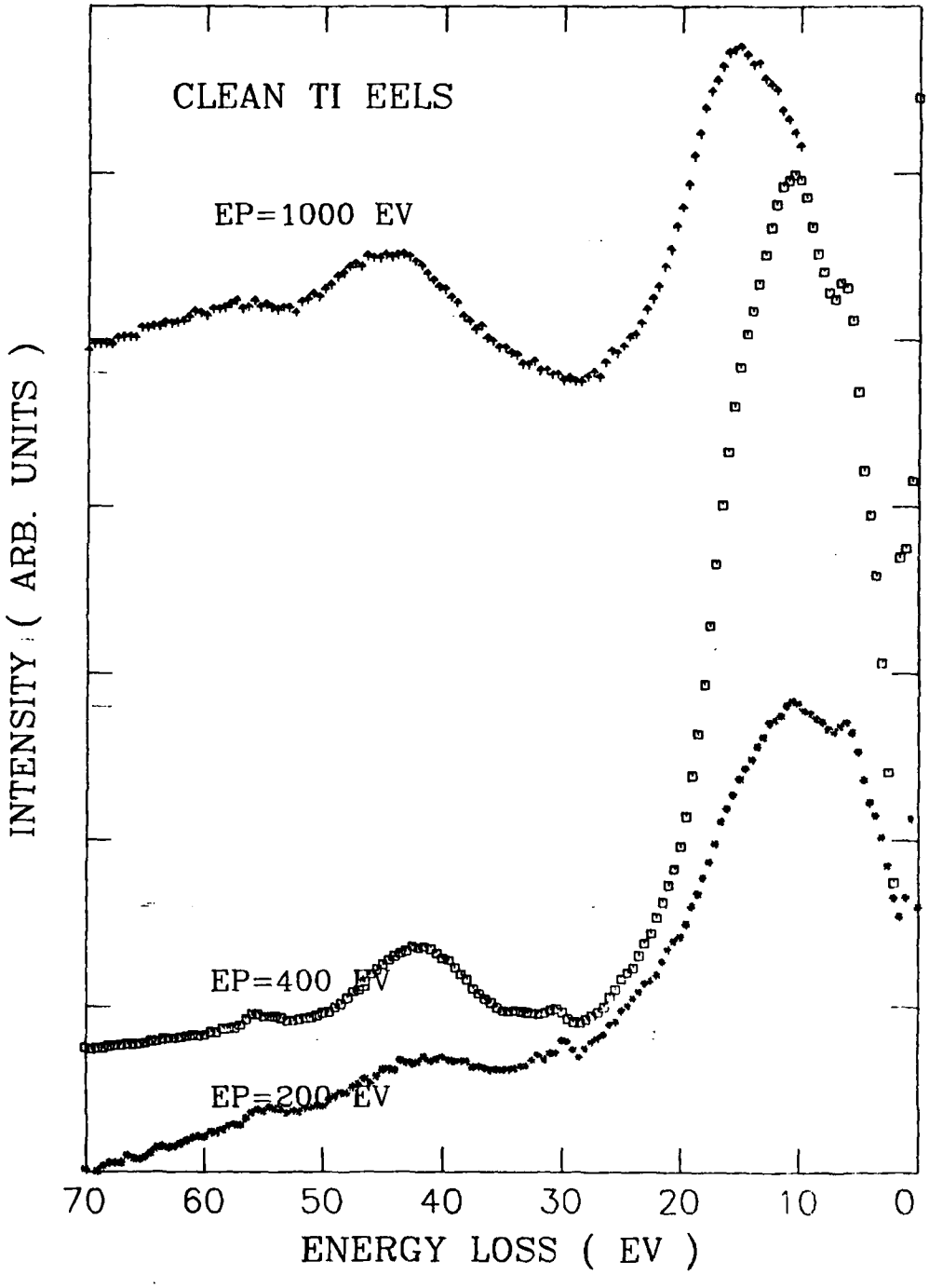

Fig.6.3. A comparison of clean Ti loss spectra for different primary energies.

The broad rise in the spectrum which peaks at about 42 eV in Fig. 6.2 is mysterious. As one can see in Fig. 3, the peak becomes more pronounced for higher primary energies. Transmission measurements for Ti (presumably partly oxidized)[6] And TiO[8] show this structure quite prominently in both the loss spectrum and the imaginary part of the dielectric function ε_2 derived from a Kramers-Kronig analysis. Its appearance in ε_2 means it is not a collective mode and must be an interband transition. A similar peak does not appear in our measurements for oxidized iron, and there are no interband losses expected in this region. No strong explanation has ever been offered for this peak, though it could be a double interband excitation or an excitation to a higher conduction band. It seems possible that the structure is connected to the metal 3p peak since it appears about 9 eV above this peak for both titanium and vanadium. It cannot be associated with an inter-band excitation of any of the oxygen states since it appears in the clean surface spectrum. A remaining possibility is that the peak is due to a collective excitation triggered by an excited 3p electron, and in this case it would presumably still appear in the ε_2 spectrum.

Our results for samples undergoing oxidation are presented in Figs. 6.4 and 6.5. Even at monolayer coverage as shown in Fig. 6.4, the surface peak is greatly reduced and the plasmon peak is seen to shift to somewhat lower energy. The O 2s peak appears at about 20 eV and continues to grow for greater oxygen coverages. The upper two curves are after several additional minutes oxygen exposure with the topmost curve being taken after no further change in the spectrum occurs. The main effect in these later spectra is that the O 2s peak and the 42 eV peak become more prominent. The sensitivity of the surface peak to contaminants or impurities makes it quite useful for surface analysis. In Fig. 6.5 we compare the oxidized spectra at EP = 200 eV and at EP = 1000 eV. There is a great change in the appearance of the spectrum below 30 eV as the plasmon peak moves to higher energy. If this movement continues for higher primary energies, the plasmon and O 2s peaks will coincide; and the spectrum will be the same as the transmission spectrum in Fig. 6.1b.

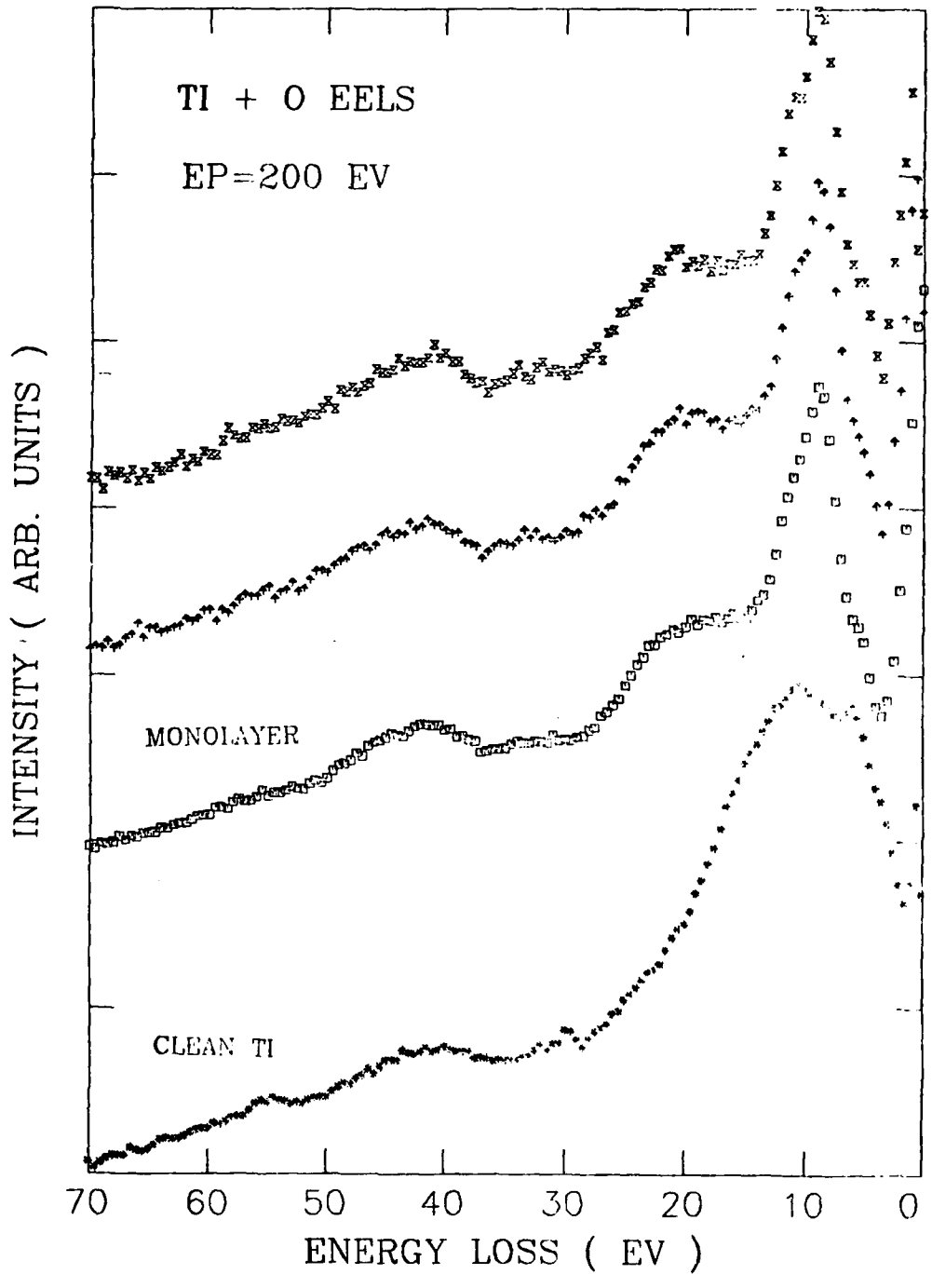

Fig.6.4. A comparison of loss spectra for clean and successively oxidized surfaces.

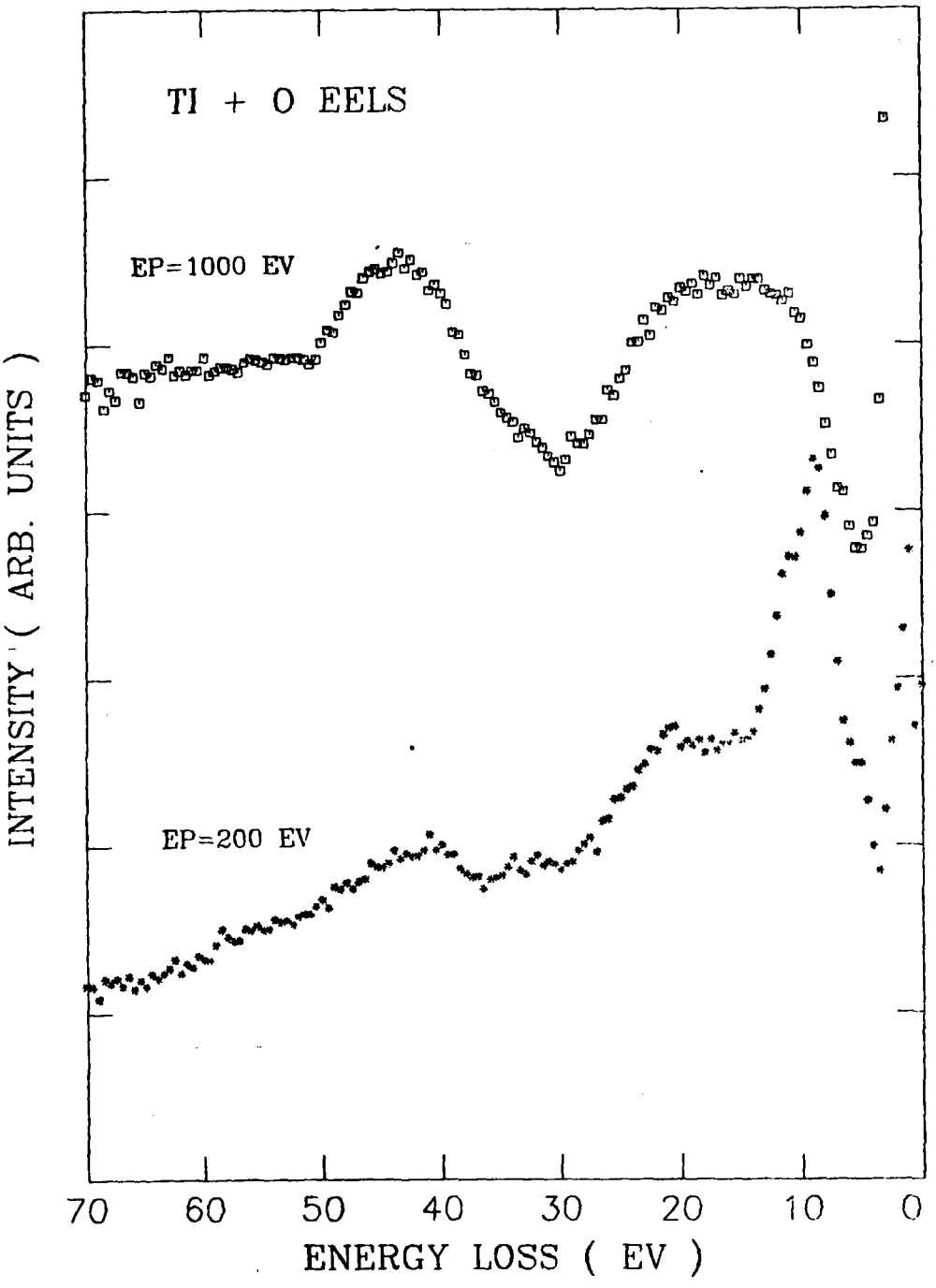

Fig.6.5. Loss spectra of final oxidized surface for EP=200 eV and EP=1000 eV.

What could cause the movement of the plasmon peak to higher energies as the incident energy is increased in the reflection experiments and also could cause the difference between the positions of the plasmon peak in the reflection and transmission experiments? A possible explanation of this movement is that it is caused by plasmon dispersion. The RPA formula for dispersion is

$$\omega_q = \omega_p\{1 + \frac{3}{10}\left(\frac{qv_f^o}{\omega_p}\right)^2 + \ldots\} \qquad (1)$$

so that non-zero momentum transfer would always result in a positive energy shift. Now in the transmission experiments,[6] the acceptance angle of the detector is 5 mrad. so that for incident energies of 35 kev the momentum spread for the electrons transmitted in the forward direction is well below the Fermi momentum. However, if there is enough scattering of the electrons within the sample, a significant number of the electrons undergoing plasmon losses and then entering the detector would transfer considerable momentum to the plasmons. We have applied to the electrons a model derived for multiple scattering of ions in a screened Coulomb region[9] and have found that the electron beam does spread enough to allow a significant number of large momentum plasmon losses to be detected. This effect would cause a shift to higher energy and a broadening of the plasmon peak. A similar effect would also take place in the reflection experiments since as the incident energy increased the electrons would penetrate deeper into the sample and be scattered more. This would explain the dependence of the plasmon peak position on incident energy.

There are evidently no measurements of the plasmon dispersion for Ti, but measurements for Aℓ indicate a dispersion of as much as 13 eV.[10] If a plasmon dispersion of several eV with a moderate increase in peak width is possible for Ti, this effect could explain the discrepancy between the transmission and reflection measurements. In that case the reflection peak would be closer to the true zero-momentum volume plasmon energy. Before any definite conclusion can be reached, however, one must do a calculation with a more realistic model of electron scattering.

These results resolve some of the conflicts between transmission and reflection loss spectra. They also reveal that care must be exercised in taking and analyzing the data. In particular for a reactive surface such as that of Ti, oxygen adsorption can greatly change the appearance of the spectrum. Our analysis provides a basis for understanding the origins of the peaks in the spectra, how they change as conditions are varied, and especially what happens to the surface peak.

VII. Implantation Damage

Because of its simplicity we have developed the electron channeling method to determine the extent of damage due to ion implantation. In this method a polycrystalline sample is placed in a scanning electron microscope and the beam rocked about the incident direction. This produces variations in the dynamical scattering and hence in the intensity of the backscattered electron signal. The technique has a spatial resolution of 10-50 μm and probes to a depth of about 500 Å, permitting the observation of damage in individual grains. We have begun to develop a technique of quantifying the channeling contrast. This is discussed in Appendix (ii).

VIII. Far Infrared Radiation as a Probe of Surface Structure and Oxidation Kinetics

For eventual use of the far infrared laser radiation as a probe of the surfaces of ion implanted titanium, it is necessary to gain some knowledge of its capabilities. As the oxidation kinetics of these materials is what is desired, data on the reflectance values of various titanium oxides in the far infrared would be of great value. A set of experiments was executed in which the reflectance values of several titanium oxides were obtained at a single wavelength over several angles of incidence. Single wavelength data was sought as under oxidation conditions, only one laser wavelength could be used because of the long lead time needed for laser set up. The resulting reflectance versus time curve could then be used to determine the state of the oxide on the surface. Far infrared wavelengths are desired for these oxidation studies because of their deep penetration of the surface.

In addition to the above measurements, a study was undertaken to evaluate the use of synchrotron radiation as an infrared source. For this work, a particular collection optics' design was analyzed numerically to determine its effect on the available infrared intensity. The motivation for this investigation was the possibility of obtaining a far infrared radiation source which would be compatible with certain types of solid state investigations (e.g. clean surface experiments, oxidation experiments).

A. Far Infrared Laser Measurements

Three different titanium oxide crystals were chosen for use in the set of far infrared reflectivity measurements to be performed using the laser. Half inch diameter polycrystalline rods of titanium monoxide (TiO), titanium dioxide (TiO_2) and titanium sesquioxide (Ti_2O_3) were obtained from Electronic Space Products, Inc. for this purpose. These oxides have the following structures in the pure state: TiO - trigonal, TiO_2 - tetragonal, Ti_2O_3 - monoclinic. To determine the purity of these oxides, the Debye-Scherrer x-ray diffraction method (i.e. the powder method) was utilized to analyze their crystalline structures. Powder diffraction patterns

were obtained using the Cu K line as a radiation source with exposure times ranging from five to six hours. From a comparison between the experimental data and the information listed in the powder diffraction file, no impurity lines were present in the diffraction patterns.

All the reflectance measurements were made at one wavelength: the 118.8 micron line of CH_3OH. Polarization measurements performed on the laser output confirmed that this line's polarization was perpendicular to that of the pumping radiation, as reported in the literature. During the experiment, several reflectance measurements were made at each angle of incidence for each titanium oxide sample. For these experiments, the range of angles spanned was 20° to 60° in 10° increments. For each power measurement (both incident and reflected), a data point was read off of the strip chart record every two seconds until approximately 30 data points were read. This sampling rate was chosen in order to take into account the response time of the detection system and the chart recorder. Each data set was corrected for drifting of the zero baseline which occurred during the measurement. For each data set, an average value was calculated which corresponded to either a reflected or incident "power" ratio depending on the data set chosen. To obtain a value for the reflectance of a particular oxide at a particular angle of incidence, the average reflected power ratio for the case of interest was divided by its analogous incident power ratio. Tables 8.1-3 list the results of these measurements.

As a result of the nature of these experiments, there is a relatively large error present in this data. A calculation of this error would be difficult, but an estimate of its value can be gained from an examination of the variance in the different calculated reflectance values for one oxide at one angle of incidence. For example, the reflectance data for TiO at 20° was found to have the following values: 80% and 88%. Therefore an error of + 5%, in these reflectance values would not be unreasonable. The sources of error in these measurements include incorrect angular positioning of the sample and detector, improper alignment of the detector, and variations in the optical path length for the reflected and incident power measurements.

Table 8.1 Reflectance Values for TiO

Angle (degrees)	Reflectance
20	.85
30	.81
40	.81
50	.79
60	.78

Table 8.2 Reflectance Values for TiO_2

Angle (degrees)	Reflectance
20	.48
30	.46
40	.41
50	.40
60	.38

The latter two are the major sources of error in the experiments. For the detector alignment, the positioning of the beam on the condensing cone influenced the output of the detector to a significant extent. Use of the aperture to center the beam helped to minimize this effect, but a slight anisotropy in the detector response was still noted. Variations in the optical path length could arise from several sources such as simply having one path length longer than another or through a difference in the optical medium for the two beam paths (e.g. more water molecules in one path). Some of these problems can be eliminated or minimized by performing these measurements either in a dry, inert atmosphere or in vacua.

From this reflectance versus angle of incidence data, it should be possible to obtain values for the optical constants of these materials at this wavelength. Several researchers have suggested and had success with calculations based on this method [11-14]. To this end a series of computer programs were written to calculate, using Fresnel's equations, the optical constants of these materials. In particular, three programs were written: one to calculate isoreflectance values, one to calculate the intersection point of two isoreflectance curves, and one to compute reflectance values for a given pair of optical constants. After testing the programs against results obtained in other researches, our reflectance values were substituted into the programs. The obtained results were less than satisfactory as it soon became clear that highly accurate reflectance was required. A brief numerical study was undertaken to determine to what extent this requirement held for this procedure. The determination of the optical constants depends on the intersection of two isoreflectance curves which were, in turn, calculated from Fresnel's equations using two of the measured values of the reflectance and angles of incidences. For steep angles of intersection, a slight change in a reflectance value (or in an angle of incidence) creates a correspondingly small change in the intersection point. Thus, in this case, optical constants may be calculated even if the reflectance data is inaccurate. For shallow angles of intersection, the intersection point is extremely sensitive to the accuracy of the reflectance data. A slight change in the "true" reflectance value

Table 8.3 Reflectance Values for Ti_2O_3

Angle (degrees)	Reflectance
20	.53
30	.44
40	.41
50	.40
60	.36

will cause the intersection point to move over a large range and even into physically unrealizable values of the optical constants. Examination of the isoreflectance data for our data showed that the angles of intersection were extremely shallow. Thus, the requirement of highly accurate reflectance data becomes clear. Further computer calculations revealed that the angle of intersection between two isoreflectance curves was more sensitive to the value of the reflectance than to the angle of incidence. That is, for high values of the reflectance (>.6), the isoreflectance curves have very large slopes for very low values of the index of refraction, n, and the extinction coefficient, k. Therefore the angle of incidence between two such curves will tend to be shallow as was the case with our data. In addition, the best chance of obtaining the optical constants using this method was found to be when the optical constants had relatively low values, $n<5$ and $k<5$. This is equivalent to stating that the reflectance values must lie below approximately .4 for all angles of incidence less than 70^{o}. Thus, this method has very limited use in the determination of the optical constants.

A final result from our far infrared reflectance measurements was the determination of the output power of the laser at the 118.8 micron line of CH_3OH. As this is one of the stronger far infrared emission lines, this would provide a comparison point for the synchrotron radiation calculations. From our measurements, the highest detector signal registered for the laser line was approximately 25 mv, but, in general, values for this signal were closer to 10 mv. Using these two figures and the voltage responsivity of the detector (i.e. .25 V/W (5)), an estimate can be obtained of the output power available from the laser. Carrying out the calculation revealed that the output power of the laser was typically about 2.5 milliwatts with the highest power output reaching approximately 6.3 milliwatts. These values are substantially lower than the values reported in the literature, indicating that the laser has not yet been optimized.

B. Synchrotron Radiation Calculations

Computer calculations were used to generate a feasibility study for the

parasitic utilization of the infrared radiation emitted by a synchrotron. A major concern with such a utilization is the presence of the higher energy radiation (e.g. X-ray and ultraviolet wavelengths) in the synchrotron radiation spectrum. The basis for this study came from earlier calculations(15) which indicated that the wavelength dependence of the vertical angle distribution of intensity could be used to advantage. The majority of the synchrotron radiation intensity is confined to within several milliradians of the orbital plane. To illustrate this point, Brown, et.al.(16) define a useful parameter, the rms angle of radiation, to estimate the angular extent of the radiation intensity for a particular wavelength. This angle is defined in the following equation:

$$\langle\theta^2\rangle_{rms}^{1/2} = (mc^2)\left(\frac{\lambda}{5.59R}\right)^{1/3}$$

where m is the mass of the electron, c is the speed of light, R is the radius of the orbit, and λ is the wavelength. This angle is defined such that 80% of the intensity available at this wavelength is contained within this angle. Tables 8.1 and 8.2 list this angle for several wavelengths for two existing synchrotrons: Aladdin I and Aladdin II. From these tables it can be seen that the high energy radiation from x-rays to visible radiation is confined to within approximately five milliradians of the orbital plane. On the other hand, to capture the same percentage of infrared radiation, angles on the order of 25 milliradians must be intercepted. It is this disparity in the angular distribution which was sought to be exploited.

Based on these results, parasitic utilization of the synchrotron radiation was considered to be possible if the design of the fore optics was such that the central region of the radiation cone would pass through a vertical aperture between two plane mirrors. This central cone would contain a majority of the hard radiation intensity (especially x-rays and ultraviolet), and seemingly very little of the infrared radiation. Several questions related to this design such as how large a central cone must be eliminated, how much high energy radiation would be present in the reflected intensity, and what would be the decrease in the infrared intensity, all had to be considered.

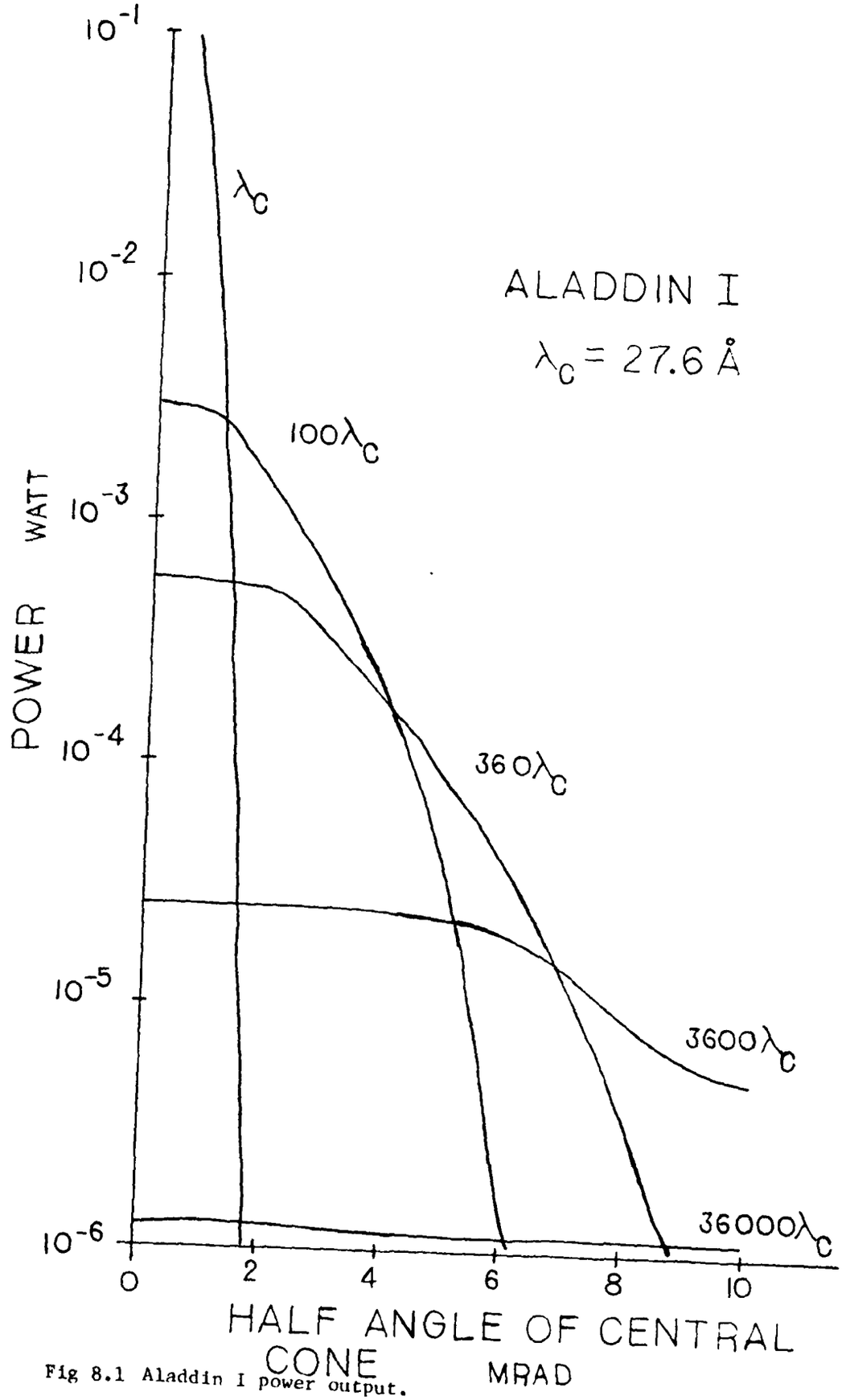

Fig 8.1 Aladdin I power output.

To answer these questions, a computer feasibility study was undertaken to analyze the problem. In this feasibility study, five synchrotron radiation machines were examined: Tantalus I, Brookhaven Vacuum UV, Brookhaven X-ray, Aladdin I, and Aladdin II. Results for the first three machines are presented in Appendix (ii) and will not be presented here. Instead, as the calculations are similar, the analysis for Aladdin I and Aladdin II will be examined and discussed. The relevant machine parameters for these calculations are given in Table 8.3.

Calculation of the synchrotron radiation intensity available at a specified wavelength when a central vertical angle was eliminated required the numerical integration of the expression for the synchrotron radiation intensity as a function of the wavelength and angle over the angles of interest. To accomplish this, a computer program was written which utilized a Simpson's rule procedure to calculate the contribution to the total intensity of a small angular differential about a specified angle. For each wavelength, the contributions from these angular segments were summed to arrive at the value for the intensity when a certain vertical angle was eliminated. Thus, if a central cone with a half angle of two milliradians was to be eliminated from the radiation pattern, the program would sum, for the specified wavelengths, only those contributions to the intensity for angles greater than two milliradians. For this study, computer calculations were performed for several values of this eliminated half angle for both synchrotron machines.

One can derive an expression for the power radiated P' by the synchrotron into a horizontal angles of $\Delta\phi$ at a fixed resolution r using the analysis given in Appendix (ii). Figures 8.1 and 8.2 are plots of P' (i.e. assuming $r\Delta\phi = 1$) as a function of the central vertical half angle of radiation which is eliminated for Aladdin I and Aladdin II respectively. Curves for several different wavelengths spanning the x-ray to infrared regions are plotted. From Figure 8.1 (i.e. plot for Aladdin I), it can be seen that at an angle of four milliradians all the radiation below the characteristic wavelength has been essentially eliminated. The

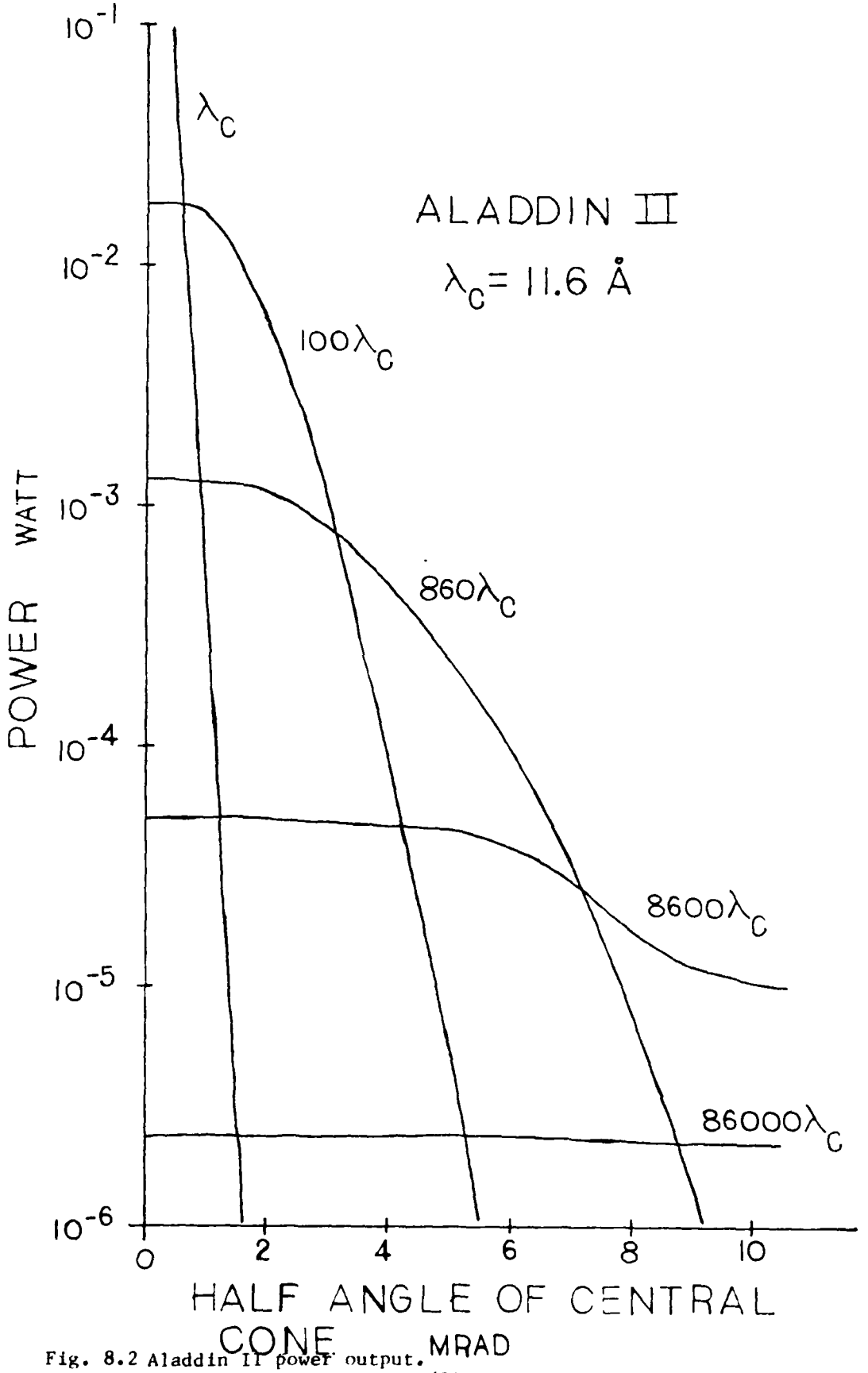

Fig. 8.2 Aladdin II power output.

peak of the intensity spectrum has shifted to the point where it now lies in the blue end of the visible spectrum. Very little of the infrared intensity has been lost as a result of this central angle elimination. For the six milliradian half angle, the intensity peak has moved into the near infrared region with only a very small decrease in the available power at the longer infrared wavelengths. In Figures 8.2 (i.e. plot for Aladdin II), for a central angle elimination of four milliradians, the power peak has already shifted into the visible region, and virtually all of the higher energy radiation has been removed. At an angle of six milliradians, the intensity peak has shifted into the near infrared with only slight decreases in the power at the longer infrared wavelengths. The main difference between these two plots is that the Aladdin II machine produces slightly more power at all wavelengths, but the power decreases at a slightly faster rate when a central angle is eliminated. Thus, with the elimination of a central angle of the radiation cone, it is possible to virtually exclude all of the hard radiation (i.e. x-rays to ultraviolet) while suffering minor losses in the infrared power. In fact, the power loss decreases with increasing wavelength.

IX. References

1. B. B. Rath, R. J. Lederich and J. E. O'Neal, Grain Boundaries in Engineering Materials, 39 (1974): ed J. L. Walter, J. H. Westbrook and D. A. Woodford.
2. A. Kryore, S. B. Chakrabortly, E. A. Starke Jr. and K. O. Legg, Ion Implantation Metallurgy, 132 (1980); ed C. M. Preece and J. K. Hirvonen.
3. S. Spooner and K. O. Legg, Ion Implantation Metallurgy, 162 (1980); ed. C. M. Preece and J. K. Hirvonen.
4. L. Pauling, The Nature of the Chemical Bond, Cornell University Press (1972)
5. G. W. Simmons and E. J. Scheibner, J. Appl. Phys. 43, 693(1972).
6. C. Wehenkel and B. Gauthe, Phys. Stat. Solidi, B64, 515 (1974).
7. Y. Ballu, J. Lecante and H. Rousseau, Phys. Rev. B14, 3201 (1976).
8. J. Frandon, B. Brousseau and F. Pradal, J. de Phys. 39, 839 (1978).
9. F. J. Szalkowski, P. A. Bertrand and G. A. Somorjai, Phys. Rev. B9, 3369 (1974).
10. P. E. Batson, C. H. Chen and J. Silcox, Phys. Rev. Lett. 37, 937 (1976).
11. R. Tousey, J. Opt. Soc. Am., 29, 235 (1939).
12. I. Simon, J. Opt. Soc. Am. 41, 336 (1951).
13. W. R. Hunter, J. Opt. Soc. Am. 55 pt. 1, 1197 (1965).
14. D. C. Hinson and J. R. Stevenson, Phys. Rev. 159, 711 (1967).
15. Private Communication, Ralph Waniek, Advanced Kinetics, Inc.

X. Publications and Presentations

During the research period, the following papers have been published:

1. "Optical Properties of Titanium and Titanium Oxide Surfaces", William E. Wall, M. W. Ribarsky and J. R. Stevenson, J. Appl. Phys. 51, 661 (1980).
2. "Design Considerations for Parasitic Use of Synchrotron Radiation in the Infrared", James R. Stevenson and J. Michael Cathcart, Nuclear Instruments and Methods, 172, 367 (1980).
3. "A comparison between the Effects of Implantation in Ultra-Clean and Standard Vacuum Environments," K. O. Legg, M. W. Ribarsky and J. R. Stevenson, Proceedings of the Conference on Modification of the Surface Properties of Metals by Ion Implantation, Manchester England (1981).
4. "Electron Channeling in Ion Implanted Titanium", H. F. Solnick-Legg, K. O. Legg, J. M. Cathcart and J. R. Stevenson, ibid.

The following presentations have been made:

1. "Inhibitions of Grain Growth in Titanium by Ion Implantation", J. M. Cathcart, K. O. Legg, J. R. Stevenson and H. Solnick-Legg, Materials Research Society, Cambridge, Mass. November 1979.
2. "Surface Grain Growth and Oxidation in Ion Implanted Titanium", J. Michael Cathcart, Keith O. Legg and James R. Stevenson; Spring meeting, APS, Washington, DC (April 1980).
3. "Use of Synchrotron Radiation in the Infrared", James R. Stevenson and J. Michael Cathcart, Southeastern Section Meeting of the APS, Chapel Hill, N. C. (November 1980).
4. "Reflectivity of Titanium and its Oxides in the Far Infrared", J. M. Cathcart, K. O. Legg and J. R. Stevenson; March Meeting of the APS, Phoenix, AZ (1981).
5. "Oxidation Characteristics of Ion Implanted Titanium", K. O. Legg, J. M. Cathcart and J. R. Stevenson, ibid.

6. "Characteristic Energy Loss Spectra of Clean and Oxidized Titanium Surfaces", M. W. Ribarsky and K. O. Legg, ibid.

7. "Effects of Ion Implantation on the Oxidation Kinetics of Polycrystalline Titanium", J. M. Cathcart, K. O. Legg and J. R. Stevenson; International Conference on Metallurgical Coatings, San Francisco, CA. (1981).

8. "The Effects of High and Ultra-high Vacuum on the Implantation of Ti", K. O. Legg, M. W. Ribarsky and J. R. Stevenson; Conference on Modification of the Surface Properties of Metals by Ion Implantation, Manchester, England (1981).

XI. Interactions

The following interactions were made during the contract period.

1. We worked with Shiro Fujishiro on the implantation of platinum in turbine blade samples and tensile test specimens. Dr. Fujishiro is a member of the Structural Metals Branch of the Air Force Materials Laboratory at Wright Patterson Air Force Base.
2. T. Eckler of Pratt and Whitney Aircraft conducted some fatigue tests and some oxidation studies on samples our group has implanted. The communication was established by Dr. Fujishiro.
3. We have interacted closely with the Metallurgy Department, carrying out implantations and analyses in support of metallurgy programs on the application of ion implantation to increasing fatigue life and to reducing aqueous corrosion in metals.
4. K. O. Legg and M. W. Ribarsky made a trip to Wright-Patterson Air Force base in December, 1980 to talk to members of the Materials Laboratory about establishing mutual directions in implantation research.

XII. Professional Personnel

The following personnel have been involved in the research during the course of this contract.

Dr. James R. Stevenson - Professor and Principal Investigator

Dr. Keith O. Legg - Senior Research Scientist and Co-Principal Investigator

Dr. M. W. Ribarsky - Research Scientist and Co-Principal Investigator

Mr. J. M. Cathcart - Ph.D. Candidate

Mr. John M. Merboth - BS Candidate

Mr. Matthew J. Rutten - BS Candidate

Ms. Patricia L. White - BS Candidate

Ms. H. Solnick-Legg - Research Scientist (Metallurgist)

Mr. Donald Hawley - M.S. Candidate

Ms. Linda Taylor - B. S. Candidate

Appendix I

A COMPARISON BETWEEN THE EFFECTS OF IMPLANTATION IN ULTRA-CLEAN AND STANDARD VACUUM ENVIRONMENTS

K. O. Legg, M. W. Ribarsky, J. M. Cathcart and J. R. Stevenson

School of Physics
Georgia Institute of Technology
Atlanta, Ga. 30332 USA

Implanting metals under the rigorously clean conditions of ultra-high vacuum can produce results different from those obtained for standard vacuum implants. We discuss here the differences in segregation properties for Er implanted Ti, in which Er segregates to a carbon covered Ti surface but not to a clean one. This is examined in terms of pair bonding theory.

INTRODUCTION

It is to be expected that the surface properties of implanted materials will be affected by both the implant itself and the contamination (principally in the form of carbon) introduced during the implantation process. In order to eliminate the latter effect it is necessary to implant under clean (ultra high vacuum) conditions. In the current paper we report a study of the implantation of erbium in titanium undertaken under standard and ultra clean conditions.

EXPERIMENTAL

Slices of a polycrystalline titanium rod were annealed at 650°C for 45 min to eliminate the acicular α, leaving pure β-Ti. They were then mechanically polished, electropolished and lightly etched. Some were implanted in standard high vacuum ($\sim 10^{-6}$ Torr) and some in ultra high vacuum (5×10^{-10} - 10^{-9} Torr during implantation) with Er^+ at 100 keV and doses between 10^{15} and 5×10^{15} ion cm^{-2}. Two of the standard vacuum implants displayed a brown spot of carbon over the implanted area while one did not. Depth profiles were determined by Rutherford backscattering (RBS), using the 200 keV implanter as a source of He^{++} ions with 380-400 keV energy and a cooled silicon barrier detector.

A typical concentration profile after implantation is shown in Fig. 1 where the dose both measured during implantation and determined by RBS was 1.3×10^{15} ion cm^{-2}. The depth at the peak is 350 Å compared with the LSS prediction of 260 Å.

After the light anneal entailed in baking the vacuum system (about

150°C for 12 hrs) the carbon covered surfaces exhibited the depth profile shown in Fig. 2b. Considering that the resolution indicated by the bars on Fig. 2 is about the width of the peak this clearly represents segregation into a surface layer no more than 100 Å thick. Furthermore, the area outside the implanted region shows the same spectrum (Fig. 2a). The Er signal height corresponds to segregation of all the implanted erbium. Auger electron spectroscopy revealed only a carbon layer from the cracked carbon within the implanted area, and from air adsorbed carbon elsewhere. There was no measurable Er signal. This suggests that the Er segregated to the interface between the Ti and the C layer and rapidly diffused across the surface beneath the adsorbed carbon.

After a high temperature anneal (750°C for 18 hrs) the RBS spectrum of the implanted and unimplanted areas changed to those of Fig. 2d and c. These show re-solution of the Er from the high concentration region near the surface.

However, when the surface was clean, as with the UHV implants or even the clean HV implant, there was no evidence of surface segregation, even on annealing in UHV. The RBS profile remained unaltered from that of Fig. 1.

ANALYSIS

In order to analyze which properties may affect the segregation of Er in Ti and Ti-C systems, we apply a Bragg-Williams type pair bonding theory (1). With this model we can study the implant distribution in the first several layers of the surface region. Although the segregated implant distribution found in the experiment may be in an interface region rather than in a few layers, the analysis will tell us something about how changes in the local bonding characteristics affect the implant concentration.

For this analysis we use the pair-bonding equation developed by Williams and Nason (2). The equilibrium concentration is found by minimizing the free energy

$$F = U - TS \tag{1}$$

with respect to concentration. Under the constraint that the total number of atoms in the system is fixed, the equilibrium condition for a binary system, AB, is

$$\frac{dF}{dx_i} = \frac{dF}{dx_b} \tag{2}$$

where x_i is the concentration of component A ($1 - x_i$ for B) in the i^{th} layer parallel to the surface, and x_b is the bulk concentration. If one uses the usual assumptions of the quasi-chemical approach (1), the enthalpy per bond of pair-bonded A is $H_{AA} = 2(\Delta H_A)_V/Z_A$ where $(\Delta H_A)_V$ is the heat of vaporization and Z_A is the number of nearest neighbors. The enthalpy per bond for B is $2(\Delta H_B)_V/Z_B$. The enthalpy associated with the AB bond is then $H_{AB} = \Omega + 1/2(H_{AA} + H_{BB})$ which is assumed concentration-independent. For the ideal solution $\Omega = 0$, and in general Ω is related to the heat of mixing of A and B. Now a simple model for relaxation can be added to this picture by assuming

$$H^r_{AA} = H_{AA}(1 + \delta), H^r_{AB} = H_{AB}(1 + \delta), H^r_{BB} = H_{BB}(1 + \delta) \tag{3}$$

in the surface layers. Here we assume that only the first layer lateral

and vertical bonds are relaxed.

One can show (2) that the resultant equations from Eq. (2) using the pair-bonding approach are

$$0 = -2\Omega[ZX_b - (1+\delta)Z_1X_1 - (1+\delta)Z_vX_2 + \frac{\delta}{2}Z_1 + \frac{\delta-1}{2}Z_v] + \Delta H_{sub}\frac{(Z_v - (Z_1+Z_v)\delta)}{Z} + kT\ln\frac{X_1(1-X_b)}{X_b(1-X_1)},$$

$$0 = -2\Omega[ZX_b - Z_1X_2 - (1+\delta)Z_vX_1 - Z_vX_3 + \frac{\delta}{2}Z_v] + \Delta H_{sub}\frac{-\delta Z_v}{Z} + kT\ln\frac{X_2(1-X_b)}{X_b(1-X_2)}.$$

$$0 = -2\Omega(ZX_b - Z_1X_2 - Z_vX_4) + kT\ln\frac{X_3(1-X_b)}{X_b(1-X_3)},$$

$$\vdots$$

$$0 - 2\Omega(ZX_b - Z_1X_N - Z_vX_{N-1} - Z_vX_b) + kT\ln\frac{X_N(1-X_b)}{X_b(1-X_N)} \qquad (3)$$

$$\Delta H_{sub} + (\Delta H_A)_V - (\Delta H_B)_V$$

where one assumes that the N + 1 st layer has a bulk composition. In Eqs. (3) Z_1 is the number of nearest neighbors in the lateral plane, and Z_v is the number of nearest neighbors in the next plane above so that $Z = Z_1 + 2Z_v$.

The effect of second nearest neighbors can be important. We can take the enthalpy of the second nearest neighbors as a fraction of the enthalpy of the first nearest neighbors. We assign the fraction a representative value of one-half in our case. Thus we can use Eqs. (3) replacing Z, Z_1 and Z_v with

$$Z_{eff} = Z + \frac{1}{2}Z_2 \quad Z_{1eff} = Z_1 + \frac{1}{2}Z_{21} \quad Z_{veff} = Z_v + \frac{1}{2}Z_{2v}.$$

In the following calculations we use these effective coordination numbers. One solves Eqs. (3) simultaneously to find the layer concentrations. We have found that it is usually not necessary to consider more than 5 layers except for certain large values of ΔH_{sub}.

The pair-bonding approach including the effects of relaxation and ordering has been studied extensively, (2-4) and we will not reproduce the composition curves for our system here since they are similar to the general curves. For ideal systems ($\Omega = 0$), the general result is that the component with the lower heat of vaporization segregates. If $\Omega > 0$ a cross-over may occur (5) so that if $(\Delta H_A)_V > (\Delta H_B)_V$, component A will segregate as X_A approaches 1 and component B as X_A approaches 0.

The parameters used in these calculations are given in Table I. Since Er and Ti are both hexagonal, $Z_A = Z_B$. Since the heat of vaporization for Ti is greater than that for Er, in the ideal case one expects Er to segregate.

The bulk composition $X_B = .99$ was calculated using the implantation dose and the implant distribution. The distribution is not uniform, of course, and X_b represents an average value. We have considered an effective number of nearest neighbors appropriate to the Ti (0001) surface. In our polycrystalline samples, crystallites with other surface planes were also exposed, but the concentration profiles will not be qualitatively different. We use heats of formation rather than heats of vaporization here since in most cases the values are close. There is no information on the heat of formation of Er - Ti, but it is known that the system is almost completely immiscible at most compositions (6). This means $\Omega < 0$. With the Er - Ti parameters almost complete segregation of Er should occur in this case. For $\Omega = 0$ the first layer Ti composition is $X_{Ti} = 1.5 \times 10^{-5}$, and for $\Omega < 0$ X_{Ti} is essentially zero. The effect of inward relaxation on the surface layer for a small positive value of Ω is shown in Table II. We see that the effect of relaxation is pronounced and that a rapid increase in Ti occurs for δ between .3 and .36. Single crystal Ti shows small relaxation in the basal plane and one would expect $\delta < .1$. However, the polycrystalline sample has many crystal orientations and there may be stronger relaxation or even reordering. Another possible effect is ordering. This effect might be important for Er - Ti since the room-temperature solid solution consists of discrete particles of essentially pure Er distributed in Ti (6). Ordering can be added to Eqs. (3) by dividing the crystal planes into sublattices (3) which have different probabilities of occupation. The order parameters is then $n_i = P^A_{\alpha,i} - P^A_{\beta,i}$ where $P_{\alpha,i}$ is the probability of occupation in the α sublattice of the i^{th} plane. The inclusion of ordering modifies only the log terms in Eqs. (3) (3) and for random alloys $n_i = 0$ and the equations reduce to Eqs. (3). It is unclear what form the ordering might take in the Er - Ti system, but we have done some preliminary calculations with a range of ordering values. The general trend is that ordering suppresses segregation. We also note that Eqs. (3) are temperature-dependent and that the effect of raising the temperature is to suppress segregation.

For a C - Er system we have the stable bonding system Er_2C which is in a distorted FCC structure (rhombohedral).(7) The difference $\Delta H_{sub} = 95.5$ kcal/mole is much larger than for Er - Ti. However, since a stable compound is formed we have $\Omega > 0$. We can estimate the value of Ω from the Pauling electronegativity scale. According to Pauling (8), the contribution of the bond to the heat of formation is $\Omega = 23\ (Y_{Er} - Y_C)^2$ where Y_{Er} is the electronegativity of Er. This formula gives $\Omega = 45.1$ kcal/mole. With these parameters we will still have quite strong segregation of Er in C for small concentrations of Er.

The effect of C adsorption on Ti can be included in our model (2). If the enthalpies per bond between adsorbing species M and A and B are H_{M-A} and H_{M-B}, respectively, then for strong adsorption we may replace ΔH_{sub} in Eqs. (3) by

$$\Delta H_{eff} = \Delta H_{sub} - (Z/Z_v)(Z_A H_{M-A} - Z_B H_{M-B}) \qquad (4)$$

where Z_A and Z_B are the coordination numbers of the A and B atoms at the surface with M. From the electronegativities (8), we see that the Ti - C bond energy contribution is only 23 kcal/mole and $\Delta H_{eff} > \Delta H_{sub}$. The C will preferentially pull the stronger bonding alloy component to the surface which is Er in this case. For example, for $\delta = .36$, the X_{Ti} drops from .94 to 10^{-2} when chemisorption of C is included.

DISCUSSION

The results of our calculations show that a mechanism such as surface relaxation, ordering, or the changes of bond energies with composition or structure must occur to prevent Er from segregating in clean Ti. Large effects due to ordering seem more likely than large relaxation effects. The bond energies may change at the surface and, indeed, may be different than in the bulk alloy since the implant distribution is certainly non-equilibrium. It is unknown how much the bond energies differ from the bulk values in the implanted system. For the Er - C system the above approach predicts strong Er segregation. For the dirty surface, a C distribution gradient into the bulk would exist due to collisions with Er ions. Since the C - Er bond energy is greater than the Er - Er or Er - Ti bond energy, this gradient would act to pull the Er to the surface. The calculation indicates the Er would tend to concentrate strongly at the surface in the presence of C. Since Er also would segregate in C, it would tend to remain at the interface rather than diffuse into the C. This is what is seen experimentally.

Other effects may contribute to this phenomenon. For example, a Ti - Er - C complex may form in the interface region or a stable TiC phase. We are planning more experiments to look at these possibilities and also at the distribution of Er in the surface region under various conditions. Also, it is clear from the above discussion that bulk quantities are inadequate and a microscopic theory should be used. Such a theory has been worked on (5) and we are presently studying ways to include microscopic calculations of bonding in this formulation.

REFERENCES

1. R. A. Swalin, Thermodynamics of Solids (Wiley, New York, 1962).

2. F. L. Williams and D. Nason, Surface Science 45, 377 (1974).

3. J. L. Moran-Lopez and K. H. Benneman, Phys. Rev. B 15, 4 769 (1977).

4. J. L. Moran-Lopez and L. M. Falicov, Phys. Rev. B 18, 2542 (1978).

5. G. Kerker, J. L. Moran-Lopez and K. H. Benneman, Phys. Rev. B 15, 6 38 (1977).

6. R. L. Beck, U. S. At. Energy Comm. LAR-10, 60 (1960).

7. G. Dean, R. Hallement, R. Lorenzelli and R. Pascard, Compt. Rend. 259, (1964) 2442-2444.

8. Linus Pauling, The Nature of the Chemical Bond, pg. 92 (Cornell Univ. Press, Ithaca, 1973).

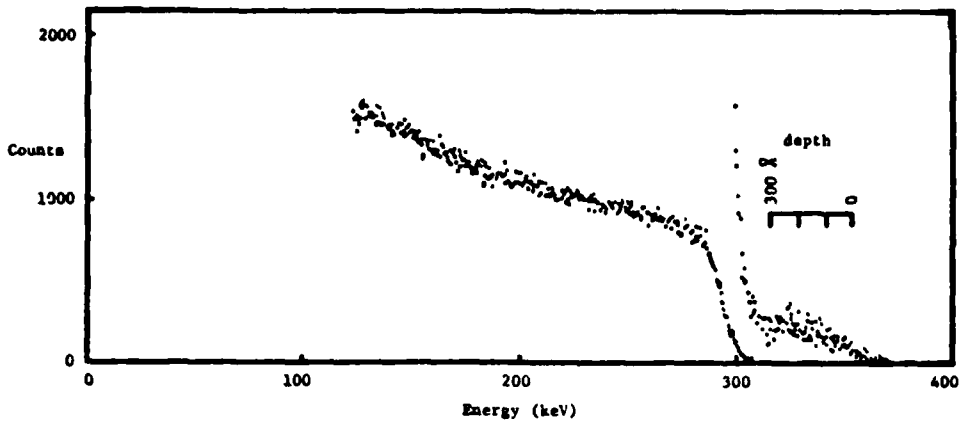

Figure 1. RBS profile of clean Er-implanted Ti (1.3 x 10^{15} ion cm^{-2} at 100 keV) using 190 keV He^{++} as a probe.

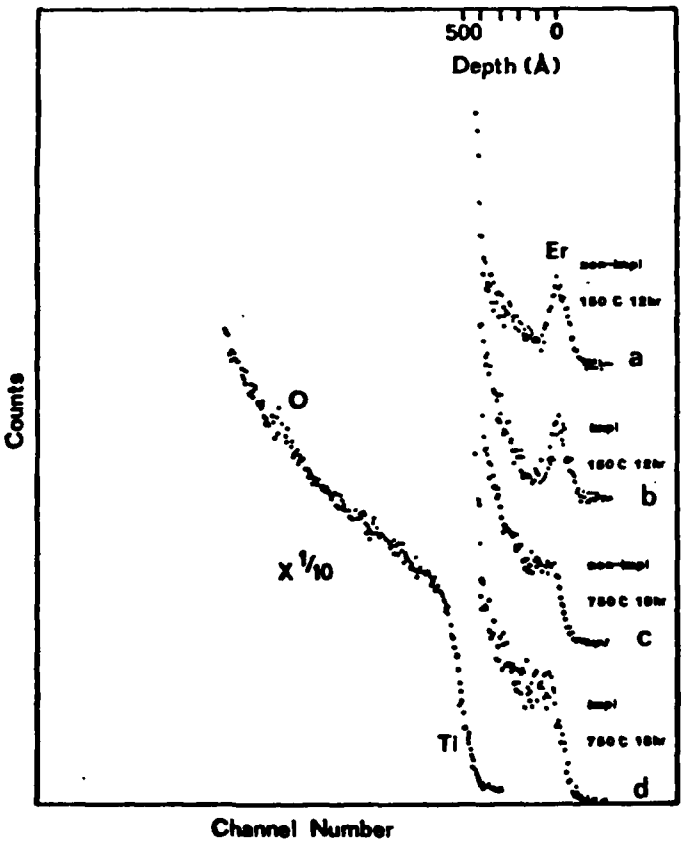

Figure 2. RBS profiles of carbon covered Er-implanted Ti inside and outside the implanted region. Annealing times and temperatures are shown on each curve.

Table I. Values of parameters used in the surface composition calculation for the Ti - Er (0001) surface at T = 300°K.

Nearest Neighbors	Effective Neighbors
$Z = 12$	$Z = 14$
$Z_1 = 6$	$Z_1 = 6$
$Z_v = 3$	$Z_v = 3$

Heats of Formation (kcal/mole)

$H_{Ti} = 112.3$ $H_{er} = 75.8$ $H_c = 171.3$

Table II. Effect of inward relaxation of first layer composition for $\Omega = -.15$ kT.

δ	.15	.18	.2	.3	.36	1.
X	.00001	.0005	.001	.124	.935	1.0

Appendix II

ELECTRON CHANNELING IN ION IMPLANTED TITANIUM

H. F. Solnick-Legg, K. O. Legg, J. M. Cathcart
and J. R. Stevenson

School of Physics
Georgia Institute of Technology
Atlanta, GA 30332 USA

Most methods of obtaining estimates of damage in implanted materials are rather cumbersome and difficult to use. An electron channeling technique is discussed which allows semi-quantitative estimates of damage in polycrystals using a scanning electron microscope. The technique is demonstrated by implants of Ti, Ar and N in titanium. Approaches to quantifying the method are discussed and illustrated.

INTRODUCTION

Selected area electron channeling provides a technique that enables many researchers to readily assess deformation in polycrystalline material using equipment widely available. In a properly equipped scanning electron microscope (SEM) the electron beam can be made to rock about a point on the specimen surface, generating an electron channeling pattern (ECP) which consists of intersecting bands and fine lines as the rocking angle intersects the Bragg angle. The varying contrasts in the ECP's are due to the differences in the emitted electron intensity as the beam sweeps through the Bragg reflections (Newbury, SEM/74). For a polycrystalline metal, if the electron beam area on the specimen can be made very small (10 μm or less) while it is rocked through the desired range of angles, a selected area channeling pattern (SACP) can be generated from a single grain. This electron channeling effect observed in the SEM has become increasingly popular as a means of determining crystallographic orientation in polycrystalline material, as well as local strains, and local dislocation densities for specimens undergoing failure analysis (Spencer et al., SEM/74).

In the initial application of this method to deformation studies (Stickler et al., SEM/71) it was found that the relationship between the pattern resulution of the SACP (defined as the angular width of the finest resolvable lines) and the dislocation density could be expressed as $W = A \log D + B$ where W = pattern resulution, D = dislocation density, and A and B are constants. The authors concluded that the SACP method is a powerful one for obtaining crystallographic and qualitative information about the degree of (crystal) deformation with the SEM. Subsequent papers presented refinements of the technique in terms of the exact experimental

conditions required to generate good SACP's (Newbury, SEM/74) and the correlation between dislocation densities and SACP resolution (Spencer et al. SEM/74). Deformation analysis using this method generally involves the careful preparation of a series of progressively deformed specimens, photographing the SACPs, determining pattern resolutions and correlating this information with the dislocation density for each sample. In the present work it is proposed to apply this technique to the study of the effects of damage done by ion implantation in the surface layers of pure Ti specimens. We will also attempt to further refine the method by analyzing the rocking (or channeling) curves generated in the SEM.

EXPERIMENTAL

Rods of Marz grade polycrystalline titanium were sliced to 2 mm thickness, annealed at 650°C for 45 min to remove acicular α, mechanically polished, electropolished and then given a light etch. Ion implantation was carried out at 100 keV, and the samples were then lightly re-etched to remove surface contamination. Selected area electron channeling patterns were generated in a JEOL-100 C electron microscope with a ASID4D attachment, operating at 80 kV accelerating voltage. The high voltage was chosen to provide a probing depth of several hundred Angstroms. Rocking angles available are $\pm$ 5° to $\pm$ 30° although most of our work was done at $\pm$ 10° or $\pm$ 15°. The signals for the rocking (or channeling) curves were obtained directly from the preamplifier of the backscattered electron detector which was a Si p-n junction type.

RESULTS

Figures 1 and 2 give SACP's for unimplanted and implanted Ti specimens. As is to be expected there is a general deterioration in the quality of the patterns as implant dose is increased. Figure 3 shows the increase in pattern line width with increasing implant dose. Typical channeling curves for self-implanted Ti are shown in Figure 4. These are merely the intensity as a function of angle along a line across the SACP. If the data from these curves is plotted as contrast (peak height/background) versus implantation dose, a curve such as that in Figure 5 results.

In Figure 6 are SACP's from Ti samples implanted with N^+ or N_2^+. Measurements showed that there was no significant difference in SACP resolution between the two implants.

DISCUSSION

A definite qualitative correlation exists between increasing ion implantation dose (damage to the surface layer) and the resolution of the SACP's. Lines on the patterns broaden and become more diffuse with increasing implant dose, while contrast deteriorates until lines are no longer discernible. The number of lines visible also decreases with increasing lattice damage, high order reflections disappearing first (Spencer et al., SEM/74). It has previously been reported (Newberg, SEM/74) that crystalline imperfections due to residual strains in the surface layers will greatly degrade the channeling pattern, thus it is to be expected that a similar effect should be found in the SACPs of ion implanted metals. Also as anticipated, the degree of crystalline imperfection created by Ar implantation in Ti was less than that due to the self-implant. This is because the energy transfer is less efficient. The difference is

particularly noticeable at a dose of 3×10^{16} ions cm^{-2} (see Figs. 1 and 2).

The damage done by N_2^+ and N^+ ions in Ti appears to be essentially the same, providing the atomic dose and the energy per N atom are the same. For 10^{16} N cm^{-2}, the measured pattern resulution was 0.0035. This is considerably less than that obtained with Ar^+ or Ti^+ (see Fig. 3) and suggests that there is no overlap between the two cascades of the N_2^+ molecule.

Because the ion implantation process can deposit a carbon or carbide layer on the implanted surface, it will be important to be able to distinguish between surface contamination, which will result in poor quality patterns (Booker, SEM/71, Newburg, SEM/74) and damage to the surface layers by the implanted ions. Work is now in progress concerning this problem. Initial results indicate that one can separate damage from contamination effects. Using SACP's as a means of analyzing damage produced by ion implantation in metals will only become a viable method when it can be more accurately quantified. To do this we are presently engaged in correlating the pattern contrast and resolution with measured dislocation densities, as a function of implantation dose.

ACKNOWLEDGEMENTS

This research was supported by the U. S. Air Force Office of Scientific Research under Grant No. AFOSR-79-0011.

REFERENCES

G. R. Booker, Proceedings of the Fourth Annual SEM Symposium, IITRI, April 1971 (SEM/71).

R. Stickler, C. Hughes, G. Booker, Proceedings of the Fourth Annual SEM Symposium, IITRI, April 1971 (SEM/71).

D. E. Newbury, Scanning Electron Microscopy/1974, IITRI, April 1974.

J. P. Spencer, G. Booker, C. Humphreys, and D. Joy, Proceedings of the Workshop on Failure Analysis and the SEM, IITRI, April 1974 (SEM/74).

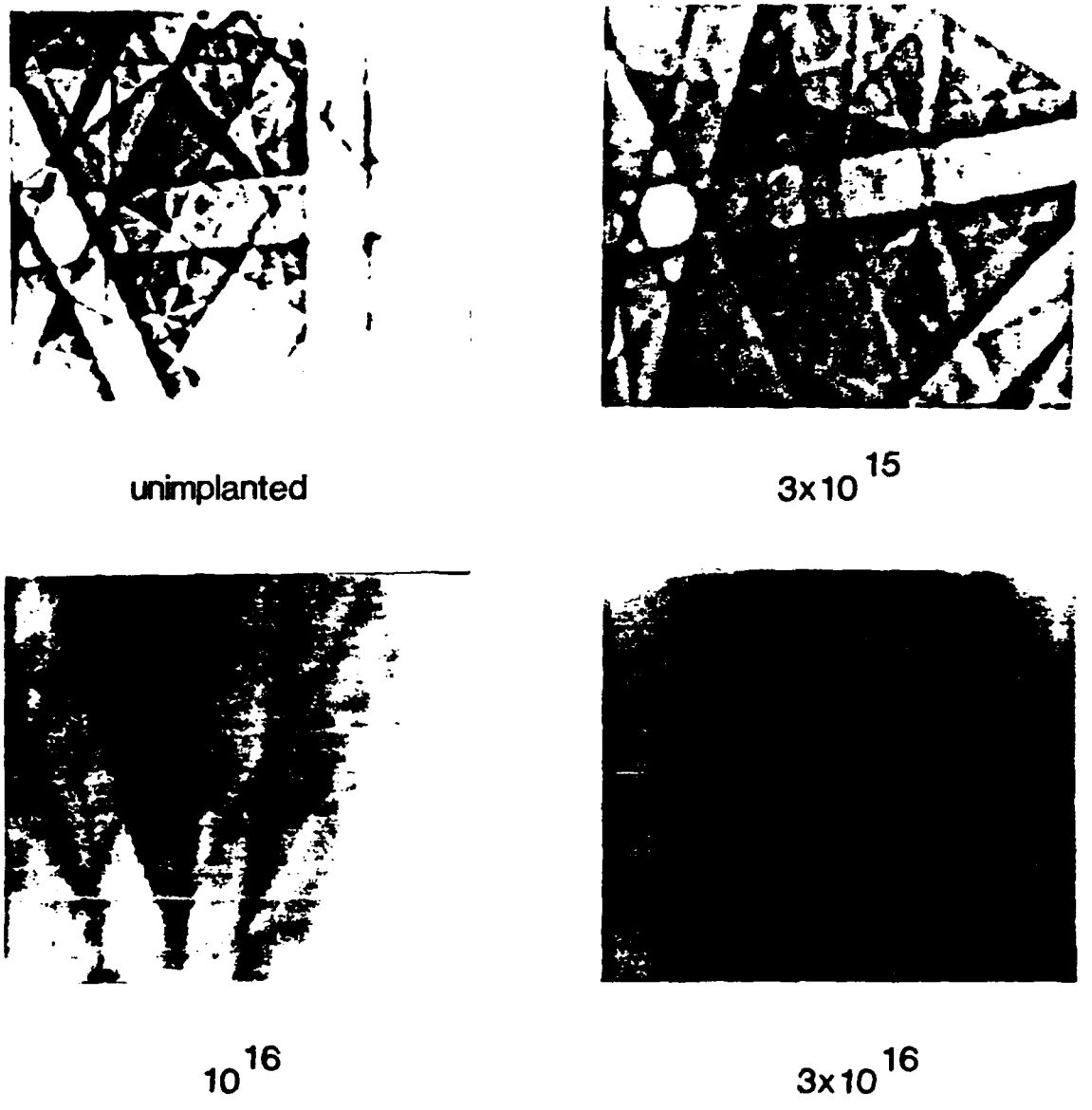

Figure 1. SACP's of 100 keV Ti^+-implanted Ti. (a) Unimplanted, (b) 3×10^{15} ion cm^{-2}, (c) 10^{16} ion cm^{-2}, (d) 3×10^{16} ion cm^{-2}.

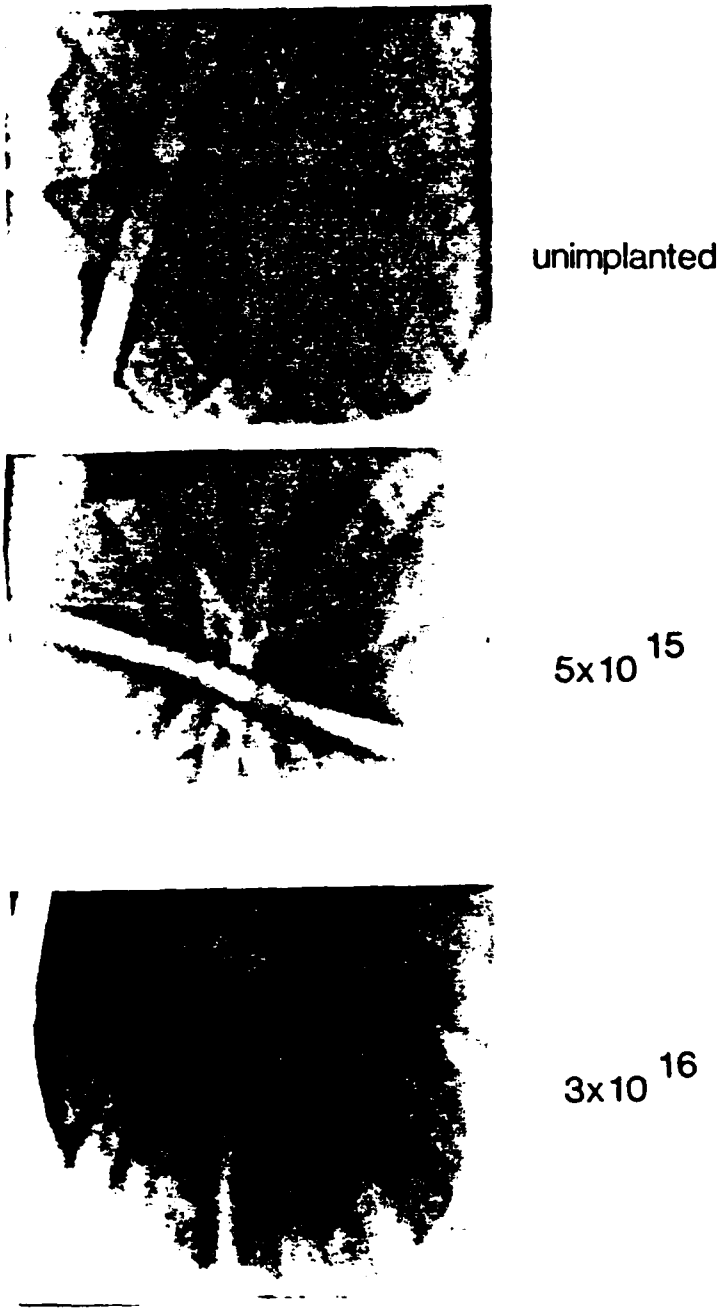

Figure 2. SACP's of 100 keV Ar^+ implanted Ti. (a) Unimplanted, (b) 5 x 10^{15} ion cm^{-2}, (c) 3 x 10^{16} ion cm^{-2}

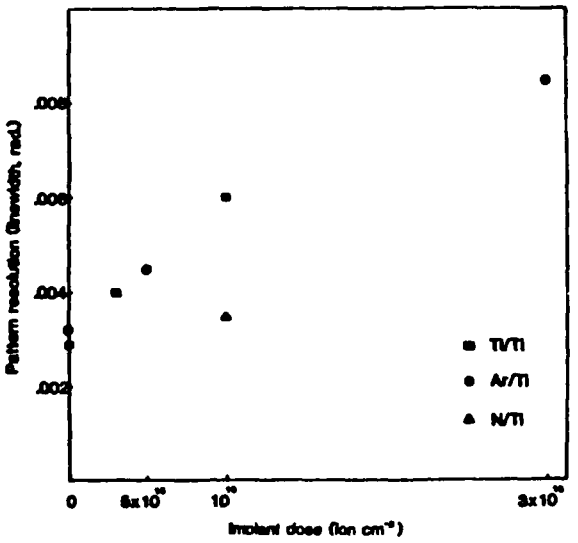

Figure 3. SACP resolution as a function of 100 keV implant dose in titanium.

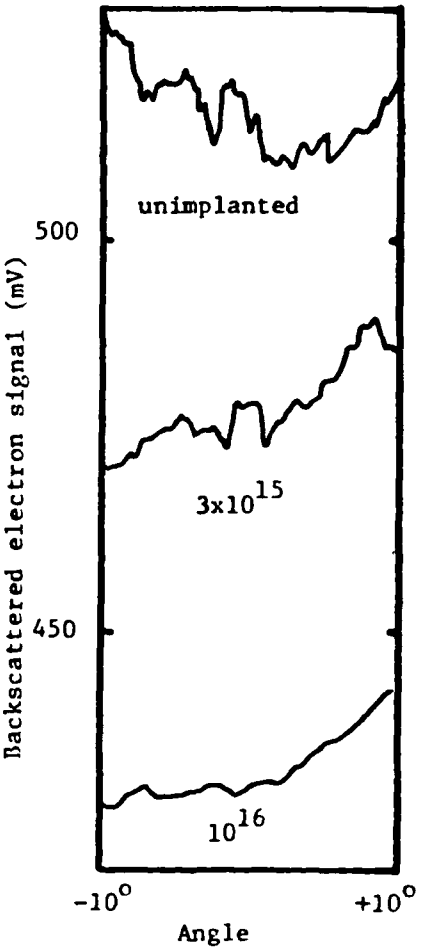

Figure 4. Typical channeling curves for 100 keV Ti^+-implanted Ti.

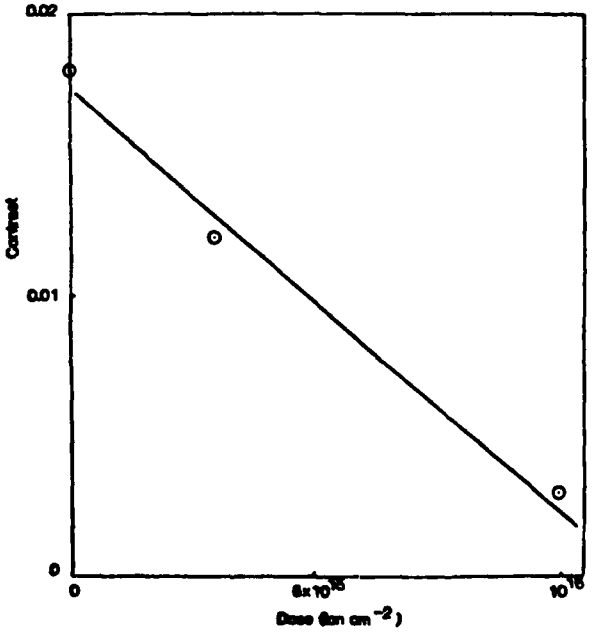

Figure 5. Contrast versus implantation dose for 100 keV Ti^+-implanted Ti.

N^+ 50keV 10^{16}

N_2^+ 100keV 5×10^{15}

Figure 6. SACP's for N implanted Ti.

Appendix III

A
Nuclear Instruments and Methods 172 (1980) 367–369

DESIGN CONSIDERATIONS FOR PARASITIC USE OF SYNCHROTRON RADIATION IN THE INFRARED *

James R. STEVENSON and J. Michael CATHCART
Georgia Institute of Technology, School of Physics, Atlanta, GA 30332, U.S.A.

Computer calculations are used to generate a feasibility study for the parasitic utilization of infrared radiation from a synchrotron radiation source. The calculations demonstrate that intercepting all but 4 to 6 mrad of the central cone will result in the hard radiation passing through an aperture with negligible loss in the intensity of the hard radiation and at the same time the long wavelength radiation will be effectively intercepted.

This approach to parasitic utilization of the infrared radiation from a synchrotron source is based on some earlier calculations [1] which indicate that the wavelength dependence of the vertical angle distribution of intensity can be used to advantage. Fig. 1 of ref. [1] gives the polarization distribution of intensity as a function of vertical angle from a synchrotron source with parameters characteristic of Tantalus I at the University of Wisconsin. As noted previously, a striation of the polarization appears as one departs from the orbital plane. In the example above, the radiation between 0 mrad and 4 mrad from the vertical is 90% polarized parallel to the plane while between 12 mrad and 16 mrad the components of linear polarization parallel and perpendicular to its plane becomes almost equal.

Fig. 2 of ref. [1] shows the sum of the two components of polarization plotted for several wavelengths as a function of vertical angle. As the wavelength becomes much greater than λ_c, a larger vertical angle must be intercepted to obtain the same percentage of the available radiation. Fortunately the vertical angles necessary remain relatively small. Brown et al. [2] introduced a useful parameter called the rms angle of the radiation. Approximately 80% of the radiated power at a wavelength is included within this rms angle. Table 1 gives this characteristic vertical angle spread for various machine parameters. The table is reproduced from earlier calculations to show the range of vertical angles necessary to intercept a significant fraction of the available energy.

* Research sponsored by the Air Force Office of Scientific Research, Air Force Systems Command, USAF, under Grant No. AFOSR-79-0011.

Using the previous results the present investigators considered a parasitic utilization of the infrared by design of the fore-optics to allow the central region of the radiation cone to pass through an aperture between two plane mirrors in the vertical plane. The central cone allowed through the aperture would contain almost all of the hard radiation but only a small percentage of the infrared. Our computer program was modified to allow the calculation of the integrals of the MacDonald functions in which the contribution from a central vertical angle can be eliminated. Obviously the data generated is quite extensive and the authors will be willing to provide more detailed compilations of the data on request.

Tables 2, 3 and 4 present a summary of the data for three different synchrotron radiation sources. Table 2 is approximately characteristic of Tantalus I, table 3 has used design parameters from the Brookhaven vacuum ultraviolet storage ring and table 4 is characteristic of the design parameters for the high energy Brookhaven machine. For fixed resolution the intensity can be written as

$$I' = 4.94 \times 10^{15} G\left(\frac{\lambda_c}{\lambda}\right) J \frac{(E)^7}{R^2} \lambda^2 F_2 r \,. \qquad (1)$$

Aside from the $G(\lambda)$ term in eq. (1), we define a multiplicative factor characteristic of machine parameters as

$$M = (4.94) \times 10^{15} J(\text{in MA}) \frac{(E \text{ in GeV})^7}{(R \text{ in meters})^2} \qquad (2)$$

Table 5 summarizes these machine dependent parameters for the three installations used in tables 2, 3 and 4. The numbers in each of these tables are a result of multiplying the factors $MG(\lambda)$. Another con-

Table 1
Angular spread of synchrotron radiation for some storage rings.

λ in units of λ_c	$\langle\theta^2\rangle^{1/2}$, Tantalus I, E = 240 MeV, γ = 471, R = 0.65 m	$\langle\theta^2\rangle^{1/2}$, DESY, E = 3 GeV, γ = 5880, R = 50 m	$\langle\theta^2\rangle^{1/2}$, Tantalus II, E = 1.76 GeV, γ = 3500, R = 4.5 m
λ_c	2.1 mrad, λ = 262 Å	0.17 mrad, λ = 10.5 Å	0.28 mrad, λ = 4.6 Å
$10^2\lambda_c$	9.8 mrad, λ = 2.62 μm	0.79 mrad, λ = 1050 Å	1.32 mrad, λ = 460 Å
$10^3\lambda_c$	21 mrad, λ = 26.2 μm	1.7 mrad, λ = 1.05 μm	2.8 mrad, λ = 4600 Å
$10^4\lambda_c$	45.7 mrad, λ = 262 μm	3.66 mrad, λ = 10.5 μm	6.14 mrad, λ = 4.6 μm

Table 2
Intensity dependence on elimination of central vertical angle for machine characteristic of Tantalus I.

Angle (mrad)	λ_c	1 μm	10 μm	100 μm
0	1.35×10^{7}	1.32×10^{6}	1.43×10^{5}	1.45×10^{4}
2	3.07×10^{6}	1.25×10^{6}	1.42×10^{5}	1.45×10^{4}
4	2.83×10^{3}	1.01×10^{6}	1.37×10^{5}	1.44×10^{4}
5	2.67	8.47×10^{5}	1.33×10^{5}	1.44×10^{4}
6	1.14×10^{-4}	6.52×10^{5}	1.29×10^{5}	1.43×10^{4}
7	1.20×10^{-10}	4.58×10^{5}	1.23×10^{5}	1.42×10^{4}
8	1.61×10^{-18}	2.88×10^{5}	1.17×10^{5}	1.40×10^{4}

Table 3
Intensity dependence on elimination of central vertical angle for machine characteristic of Brookhaven Vacuum U.V. Design.

Angle (mrad)	λ_c	1 μm	10 μm	100 μm
0	4.64×10^{7}	6.54×10^{5}	6.68×10^{4}	6.71×10^{3}
2	3.99×10^{-3}	5.80×10^{5}	6.53×10^{4}	6.68×10^{3}
4	7.65×10^{-67}	3.39×10^{5}	6.04×10^{4}	6.58×10^{3}
5	1.18×10^{-135}	1.97×10^{5}	5.65×10^{4}	6.51×10^{3}
6	5.23×10^{-238}	8.90×10^{4}	5.16×10^{4}	6.41×10^{3}
7	$<10^{-288}$	2.96×10^{4}	4.57×10^{4}	6.30×10^{3}
8	$<10^{-288}$	6.89×10^{3}	3.91×10^{4}	6.17×10^{3}

Table 4
Intensity dependence on elimination of central vertical angle for machine characteristic of Brookhaven 2.5 GeV design.

Angle (mrad)	λ_c	1 μm	10 μm	100 μm
0	1.21×10^{9}	1.31×10^{6}	1.25×10^{5}	1.21×10^{4}
2	$<10^{-288}$	9.56×10^{5}	1.25×10^{5}	1.19×10^{4}
4	$<10^{-288}$	1.77×10^{5}	1.01×10^{5}	1.14×10^{4}
5	$<10^{-288}$	2.94×10^{4}	8.33×10^{4}	1.11×10^{4}
6	$<10^{-288}$	2.04×10^{3}	6.30×10^{4}	1.07×10^{4}
7	$<10^{-288}$	4.93×10^{1}	4.30×10^{4}	1.01×10^{4}
8	$<10^{-288}$	3.49×10^{-1}	2.60×10^{4}	9.46×10^{3}

Table 5
Machine parameters

	λ_c	j	r	e	m
(1) Tantalus I	262 A	100 MA	0.65 m	240 MeV	5.363×10^{13}
(2) Brookhaven UV	31.6 A	1000 MA	51.0 m	0.7 GeV	1.564×10^{14}
(3) Brookhaven X	2.48 A	500 MA	170.2 m	2.5 GeV	5.204×10^{16}

sideration is that we have assumed the entire vertical angle can be intercepted. As seen in table 1 this could pose a problem for some long wavelengths. However, as seen in previous results, the correction is probably not greater than a factor of two.

In summary, the data presented in tables 2, 3 and 4 show the feasibility of allowing the central cone having a vertical angle of 4 to 6 mrad pass through an aperture and to intercept the remaining radiation to use at longer wavelengths. The hard radiation in the vicinity of $\lambda = \lambda_c$ is effectively decreased in the intercepted beam while the light passing through the aperture has been filtered of long wavelength radiation.

References

[1] James R. Stevenson, H. Ellis and Roger Bartlett, Appl. Opt. 12 (1973) 2884.

[2] F.C. Brown, P.L. Hartman, P.G. Kraiger, B. Lax, R.A. Smith and G.H. Vineyard, Synchrotron radiation as a source for spectroscopy of solids, NRC Solid State Panel Subcommittee Rep. (Mar. 1966).